

# An Associated and Nonassociated Flow Rule Comparison for AISI 439-430TI Forming: Modeling and Experimental Analysis

O. Chahaoui<sup>a</sup> , N. Matougui<sup>\*b</sup> , S. Boulahrouz<sup>a</sup> , M. Heddar<sup>b</sup> , K. Babouri<sup>b</sup> 

<sup>a</sup> I.S.M.A Laboratory, Laghrour-Abbes University of Khenchela, Algeria. Email : oualid.chahaoui@gmail.com, boulahrouz\_salim@yahoo.fr

<sup>b</sup> L3M- École nationale supérieure des mines et métallurgie-Annaba, Algeria. Email: nedjouamaatougui@yahoo.fr, mohamed.heddar@ensmm-annaba.dz, kaouter.babouri@ensmm-annaba.dz

\* Corresponding author

<https://doi.org/10.1590/1679-78256724>

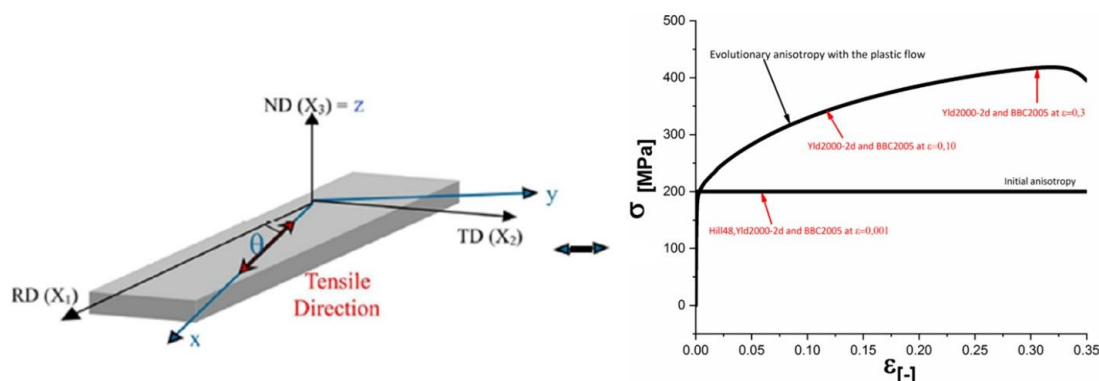
## Abstract

The plastic anisotropy behavior of ferritic stainless steel (FSS) sheets was analyzed and modeled under associated and nonassociated flow rule approaches. Three orthotropic flow functions, known as quadratic *Hill48* and nonquadratic (*Yld2000-2d* and *BBC2005*), were developed and employed under an associated and nonassociated flow rule hypothesis. For the *NAFR* based on the initial anisotropy, the mechanical behavior was described by the nonexponential model functions of *Yld2000-2d* and *BBC2005* to predict the directional dependence of mechanical parameters. It provided a considerable advantage in terms of flexibility and good agreement with the experiment. According to the results, the polynomial fit functions of the transverse versus longitudinal true plastic strain curve were used to describe the designated properties corresponding to a selected level of strain. To describe the evolution of anisotropic hardening and potential plastic hardening, seven different loading conditions were considered. The proposed evolutionary *non-AFR Yld2000-2d* and *BBC2005* criteria showed good accuracy in predicting the evolution of hardening yield and Lankford coefficients depending on the plastic deformation.

## Keywords

Yield function, Anisotropic behaviour, Constitutive model, Nonassociated flow rule, Sheet metal forming, Evolution of plastic anisotropy.

## Graphical abstract



Received September 03, 2021. In revised form September 12, 2021. Accepted September 21, 2021. Available online September 24, 2021

<https://doi.org/10.1590/1679-78256724>



Latin American Journal of Solids and Structures. ISSN 1679-7825. Copyright © 2021. This is an Open Access article distributed under the terms of the [Creative Commons Attribution License](https://creativecommons.org/licenses/by/4.0/), which permits unrestricted use, distribution, and reproduction in any medium, provided the original work is properly cited.

## 1 INTRODUCTION

Over the past few decades, Ferritic stainless steels (FSS) with approximately 17% Cr (X3CrTi17, AISI 439-430Ti; EN 1.4510) offer significant potential application in automobiles, particularly in cold end parts production, such as mufflers and tail pipes. One of the major drawbacks preventing such application is their poor formability, originating from their complex microstructures and pronounced textures (O. Chahaoui et al., 2013; Raabe and Lucke, 1993). Therefore, numerous studies have been conducted to improve the formability of ferritic stainless steels by weakening the earing phenomena induced by the crystallographic texture and the resulting elastic-plastic anisotropy of the selected metals (Benke et al., 2018; Beyerlein and Knezevic, 2018; Oh et al., 2017). The main two reasons for Textures occurrence relating to earing are as follows: (i) during thermomechanical processing, continuous recrystallization has been observed (Belyakov et al., 1998; Cizek and Wynne, 1997), which impedes any texture randomization, and (ii) upon cooling, no phase transformation may occur. Furthermore, such structural textures are not completely eliminated or even modified using subsequent cold rolling and/or heat treatments (O. Chahaoui et al., 2011).

In order to describe the mechanical features of different materials, several yield functions were proposed under the anisotropic yield function criterion. Similar to the outcome from von Mises criterion von Mises (1913) (Mises, 1913), the quadratic formulation associated with the flow rule was successfully suggested and developed by Hill (1948) (Rodney Hill, 1948); hence, this criterion was based on Drucker's postulate, as well as, the Lankford calibration parameters. Over the previous works of Barlat et al. (Barlat et al., 1997, 2003, 2005), the mechanical properties were predicted using more recent formulations from linear functions. Karafillis and Boyce (Karafillis and Boyce, 1993) modeled the anisotropic behavior of DC06 sheets under the Hill48 model. They defined the coefficients of these criteria as function of the plastic strain and successfully developed isoerror maps. Later, including in-plane anisotropy under plane stress conditions, a nonquadratic yield criterion was suggested by Banabic et al. (Banabic et al., 2003, 2005, 2000), from which, it was possible to investigate the anisotropic properties of metals that required more data for calibration. While to describe and improve the formulations anisotropy, linear transformations of the stress tensor were well used by Bron and Besson (Bron and Besson, 2004).

Moreover, Spitzing and Richmond (Spitzing and Richmond, 1984) observed that the influence of pressure on the stress in steel and aluminum alloys was not followed by the anticipated plastic expansion, as specified by the associated plasticity (AFR). Subsequently, they specified and confirmed that the AFR was not exact. In addition, many researchers (Lee et al., 2017; Stoughton, 2002) have described the material anisotropy through a new computational model, resulting in stress tensor dissociated predictions and strain ratio (*r-values*). However, incompatible phenomenological data of associated plasticity (AFR) with regard to the dependence on hydrostatic pressure (i.e., mean stress in the spherical tensor) of flow stress during classical plasticity (i.e., associated plasticity) were reported. While the nonassociated flow rule (*non-AFR*) was applied, the plastic potential was decoupled from the yield function, from which the final volume was not significant compared to that measured.

Concurrently, Stoughton and Yoon (Stoughton and Yoon, 2006) introduced a spherical stress-sensitive function under a *non-AFR* for rolling metal sheets. Taking into account this comparison between the two criteria (AFR) and (*non-AFR*), some experimental works have been initiated to identify the evolution of the mechanical parameters through metal plastic deformation using various yield criteria of plasticity, corresponding to the evolution of the flow stress and the instantaneous anisotropy coefficient. Hu, Zamiri, Darbandi (Hu et al., 2018; Darbandi and Pourboghrat, 2011; Zamiri and Pourboghrat, 2007) and more recently, Safaei et al., (2014), An, Lian and Džoja (An et al., 2013; Džoja et al., 2019; Lian et al., 2018; Safaei, Yoon et al., 2014) reported a model for computing the evolution of the local Lankford *r* coefficient according to the ISO standard. The *r-values* were calculated via linear regression for a given strain amount and polynomial fit functions. They thoroughly defined the model parameters related to the plastic strain. Thus, the model could accurately predict the evolution of Lankford *values* and hardening stresses according to the plastic deformation. However, Lian et al. (Lian et al., 2018) proposed a nonassociated Hill48 plasticity model from which the experimental and modeled anisotropy analyses were thoroughly compared using the forming limit curve (FLC) of ferritic stainless steel. Based on the above works, there is very limited works on the comparison of plastic anisotropy under associated and nonassociated flow rule for FSS steel forming.

Therefore in this study, more flexible and adaptable functions of the nonquadratic anisotropic yield criterion (*Barlat Yld2000-2d*) (Barlat et al., 2003) and (*Banabic BBC2005*) (Banabic et al., 2005) are investigated and compared. The aim is to analyse the initial mechanical anisotropy of the yield surface under AFR, combined with the isotropic hardening formulation for the surface hardening evolution under the plane stress conditions of FSS steel. It is interesting to investigate the variation in the yield locus when comparing the three yield functions (*Hill48*, *Yld2000-2d* and *BBC2005*) along different orientations in the plane sheet under *NAFR*. Thereafter, using commonly the Mechanical parameters such as the unidirectional yield stresses  $\sigma(\vartheta)$  and the strain rate ratio  $r(\vartheta)$  (the anisotropy coefficient), or the Lankford

coefficient, the plastic behavior of deformation and stress in the sheet plane is well identified, via monodirectional tensile tests applied to rectangular samples.

This study is organized as follows: First, a general framework was addressed to present an analysis of the hypothesis of plasticity (associated and nonassociated). Based on orthotropically symmetric metals, anisotropic behavior was noted in yield functions for sheet metals via mathematical formulations using two exponential functions: i) a quadratic formalism of *Hill48* and (ii) *Yld2000-2d* and *BBC2005* nonquadratic yield functions. To verify and quantify the anisotropic behavior of initiated state sheet metal relative to its orthotropic planes at the microscopic scale, quantitative microstructural analysis of ferritic stainless steel (*FSS*) was proposed. The stereological measurements were carried out at the microscopic scale using optical micrographs. Then, tensile tests were performed to compute the mechanical features of the *FSS* as required for the analysis, the instantaneous evolution of the experimental normalized yield stress associated with a specific level of equivalent deformation was computed using the Voce hardening model. After that, based on 3<sup>rd</sup> and 4<sup>th</sup> order polynomial functions, by finding the ratio curves of the transverse to the longitudinal plastic strain for 7 uniaxial directions, the anisotropic parameters of both yield functions have been optimized and compared with those modeled. Finally, the validation and discussion of prediction the mechanical behavior of the *FSS* sheet corresponding to the amounts of plastic deformation using the evolutionary *non-AFR* of the *Yld2000- 2d* and *BBC2005* anisotropic models were well highlighted.

## Nomenclature

RD, TD, DD, ND	The main directions in the plane of the sheet frame: Rolling, Transverse, Diagonal and Normal
$\lambda, \nu, \rho$	Anisotropy parameters of <i>Hill48</i> yield function
$\alpha_1-\alpha_8$	Anisotropy parameters of <i>YLD2000-2d</i> yield function
$a, b, L, M, N, P, Q, R$	Anisotropy parameters of <i>BBC2005</i> yield function
$f(\sigma_{ij}), g(\sigma_{ij})$	Yield and plastic potential functions
$S'_1, S'_2$	Components of deviator stress in the First linear transformation
$S''_1, S''_2$	Components of deviator stress in the second linear transformation
$S_1, S_2$	Deviators of stress in principal frame
$r(\vartheta)$	Anisotropic parameter (Lankford value)
$\vartheta$	The angle at which the specimen is taken in the plane of the sheet in relation to RD.
$\sigma_{ij}$	components of stress tensor
$\sigma_0$	Effective (Equivalent) yield stress
$\sigma_{ref} = \sigma_0$	Stress of reference according to rolling direction
$\sigma(\vartheta)$	Yield stress under the plane sheet
$\sigma_b$	Equibiaxial stress
$r_b$	Equibiaxial <i>r-value</i>
$\nu$	Poisson's coefficient
$\dot{\epsilon}_{ij}$	Components of strain rate tensor
$\sigma_t, \epsilon_t$	True Stress and true strain
$\beta$	Hardening coefficient
$\bar{\epsilon}^p$	Equivalent plastic strain component
$E$	Moduli of Young
$\sigma_{sat}$	Saturation stress in Voce hardening model
$m(\vartheta)$	is a gradient that measures the steepness of longitudinal and transverse direction

## 2 CONSTITUTIVE BASIC EQUATIONS OF THE NONASSOCIATED FLOW RULE

The forming of rolled sheets generally has both elastic and plastic properties. Under the consideration of the quasi-static plasticity and small deformation assumptions, the total strain rate can be partitioned additively into two parts:

1. Idealized elastic stress-strain behavior when it is represented by Hooke's law.
2. A large nonlinear deformation (plastic deformation).

$$\varepsilon^t = \varepsilon^e + \varepsilon^p, \quad \sigma_{ij} = C_{ijkl}(\varepsilon_{kl}^t - \varepsilon_{kl}^p) \tag{1}$$

where  $\sigma_{ij}$  is the Cauchy stress, and the fourth-order tensor  $C_{ijkl}$  is a material elastic stiffness value. Only the plane-stress condition is written as:

$$\begin{Bmatrix} \sigma_{11} \\ \sigma_{22} \\ \sigma_{12} \end{Bmatrix} = \frac{E}{(1-\nu^2)} \begin{bmatrix} 1 & \nu & 0 \\ \nu & 1 & 0 \\ 0 & 0 & \frac{1-\nu}{2} \end{bmatrix} \begin{Bmatrix} \varepsilon_{11} \\ \varepsilon_{22} \\ 2\varepsilon_{12} \end{Bmatrix} \tag{2}$$

$$F(\sigma_{ij}, \sigma_0(\bar{\varepsilon}^p)) \leq 0 \Rightarrow f_y(\sigma_{ij}) - \sigma_0(\bar{\varepsilon}^p) \leq 0 \text{ and } \bar{\varepsilon}_p = \int d\bar{\varepsilon}_p \tag{3}$$

The yield function  $f_y$  is also referred to as a phenomenological yield function. If  $F < 0$ , it presents the elastic domain,  $F = 0$  refers to the plastic regime and  $F > 0$  is in a nonallowed domain.  $f_y(\sigma_{ij})$  is the equivalent stress, and  $\sigma_0(\bar{\varepsilon}^p)$  is the unidirectional isotropic hardening model along the rolling direction (RD). A non-associated plastic flow rule is given as:

$$\dot{\varepsilon}_{ij}^p = \dot{\lambda} \frac{\partial f_p(\sigma_{ij})}{\partial \sigma_{ij}} = \dot{\lambda} g \tag{4}$$

Where  $f_p$  is the  $n$ -th order homogeneous potential plastic **function**. the constant  $\dot{\lambda}$  is also referred to as the plastic multiplier.  $g$  is the first gradient of the plastic function denoting the plastic flow direction.

If the yield function  $f(\sigma)$  is identical to the potential  $g(\sigma)$  function, i.e.,  $f(\sigma) = g(\sigma)$ , the assumption of an associated flow rule (AFR) is applied, and if not, the nonassociated flow rule (NAFR) is dominant. The different concepts of AFR and NAFR are illustrated in Figure 1 in normalized stress space.

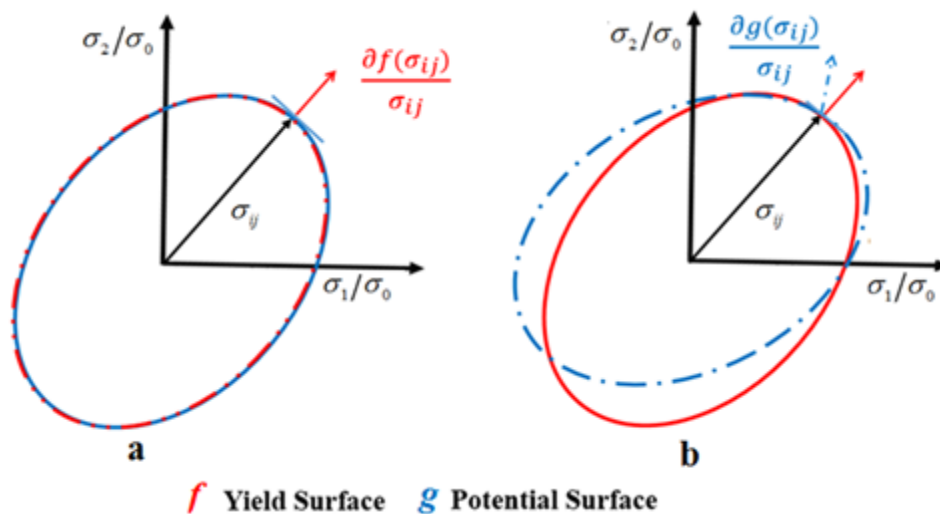


Figure 1 Schematized concepts of (a) Associated Flow Rule and (b) Non-Associated Flow Rule.

The equivalent plastic work principle is expressed by:

$$\dot{W} = f_y(\sigma_{ij}) \bar{\varepsilon}_{ij}^p = \sigma_{ij} \dot{\varepsilon}_{ij}^p \tag{5}$$

Using Euler's theory for the homogeneous first-order function of the plastic potential:

$$\sigma_{ij} : \frac{\partial f_p(\sigma_{ij})}{\partial \sigma_{ij}} = f_p(\sigma_{ij}) \tag{6}$$

The incremental strain theory is based on the concept of dissipated plastic work, with the plastic potential homogeneous functions restricted in the first order. Furthermore, Euler's theorem was applied Safaei (2014) and Hu (2018) (Cvitanic et al., 2008; Cvitanic et al., 2017; Hu et al., 2018; Safaei, Yoon, et al., 2014). Replacing relation (4) into relation (5) and applying relation (6) supplies the following:

$$\bar{\varepsilon}_{ij}^p = \dot{\lambda} \frac{\sigma_{ij} : \frac{\partial f_p(\sigma_{ij})}{\partial \sigma_{ij}}}{f_y(\sigma_{ij})} = \dot{\lambda} \frac{f_y(\sigma_{ij})}{f_p(\sigma_{ij})} \tag{7}$$

The following relation is obtained by differentiating Equation (1).

$$\frac{\partial f_y(\sigma_{ij})}{\partial \sigma_{ij}} : \sigma_{ij} = \frac{\partial \sigma_0(\bar{\varepsilon}^p)}{\partial \bar{\varepsilon}^p} : \dot{\varepsilon}^p \tag{8}$$

The Cauchy tensor deduced from the elastic constitutive law is:

$$d\sigma_{ij} = C_{ijkl} d\varepsilon_{kl}^e = C_{ijkl} (d\varepsilon_{kl}^t - d\varepsilon_{kl}^p) = C_{ijkl} : (d\varepsilon_{kl}^t - \dot{\lambda} \frac{\partial f_p(\sigma_{ij})}{\partial \sigma_{ij}}) \tag{9}$$

Using Equation (9) into relation (8) and employing Equation (6), the positive scalar  $\dot{\lambda}$  is provided as:

$$\dot{\lambda} = \frac{\frac{\partial f_y(\sigma_{ij})}{\partial \sigma_{ij}} : C_{ijkl} : \dot{\varepsilon}_{kl}^t}{\frac{\partial \sigma_0(\bar{\varepsilon}^p)}{\partial \bar{\varepsilon}^p} \frac{f_p(\sigma_{ij})}{f_y(\sigma_{ij})} + \frac{\partial f_y(\sigma_{ij})}{\partial \sigma_{ij}} : C_{ijkl} : \frac{\partial f_p(\sigma_{ij})}{\partial \sigma_{ij}}} \tag{10}$$

where for the associated flow rule  $\dot{\varepsilon}_{ij}^p \equiv \dot{\lambda}$ .

### 3 YIELD FUNCTIONS FOR SHEET METALS

#### 3.1 Hill (1948) Yield Criterion

In the current contribution, the Hill (1948) (Rodney Hill, 1948) yield function, as one of the most widely admitted models in mechanical or yield plastic potential modeling, can be given in a general formulation under plane stress conditions (i.e.;  $\sigma_{13} = \sigma_{23} = \sigma_{33} = 0$  and  $\sigma_{11}, \sigma_{22}, \sigma_{12} \neq 0$ ). The Hill48 yield function can be expressed in the following form:

$$f(\sigma_{ij}) = \sigma_{11}^2 + \lambda \sigma_{22}^2 - 2\nu\sigma_{11}\sigma_{22} + 2\rho\sigma_{12}^2 = \sigma_0^2 \tag{11}$$

The anisotropy parameters of  $\lambda$ ,  $\nu$  and  $\rho$  are generally:

- a. identified from mechanical characterization (i.e., usual unidirectional tensile test and simple shearing in plane considered)
- b. and/or discretized from texture components (O. Chahaoui et al., 2011). In the case of  $\lambda=1$ ,  $\nu=1/2$  and  $\rho=3/2$ , the *Hill48* yield criterion reduces to the Mises yield function.

Since sheet material forming is characterized by  $\sigma(\theta)$  mechanical flow stress, which is essentially related to microstructural structures, the drawability is generally related to the *r-values* (anisotropy coefficient). Based on the *Hill48* quadratic function as well as on the associated and nonassociated flow rule, the formulations determining the mechanical parameters are:

$$\sigma(\theta) = \frac{\sigma_0}{\left(\cos^4 \theta + \lambda \sin^4 \theta + 2(\rho - \nu) \sin^2 \theta \cos^2 \theta\right)^{1/2}}$$

$$r(\theta) = \frac{\nu + (2\rho - 1 - \lambda - 2\nu) \cos^2 \theta \sin^2 \theta}{(\lambda - \nu) \sin^2 \theta + (1 - \nu) \cos^2 \theta} \tag{12b}$$

### 3.1.1 Coefficients of yield stress and plastic potential function

Different methods can be used to identify and deduct these coefficients:  $\lambda$ ,  $\nu$  and  $\rho$  of the *Hill48* quadratic criterion. Two main approaches (*AFR* and *non-AFR*) can be used:

- a. **Associative flow rule (AFR):** It is noted that for the anisotropy of the sheet metal under the hypothesis of the associated plasticity rule (*AFR*), the two directions of yield stress (*Hill48-y*) and plastic strain (*Hill48-r*) are strictly parallel and this produce the same anisotropy.
- b. **Non-Associative flow rule:** In non-associated plasticity, the two directions of yield stress (*Hill48-y*) and plastic strain (*Hill48-r*) are different, and the mechanical behavior can be independently represented by two distinct anisotropies.
- c. **b1- Stress-based Hill's 48 function (Hill48-y):** The yield function requires four experimental uniaxial yield stresses corresponding to the rolling (RD), transverse (TD) and diagonal (DD) directions as well as balanced biaxial sollicitation (RD = TD). Material anisotropic coefficients can be adjusted as follows:

$$\lambda_y = \left(\frac{\sigma_0}{\sigma_{90}}\right)^2 ; \quad \nu_y = \frac{1}{2} \left( 1 + \left(\frac{\sigma_0}{\sigma_{90}}\right)^2 - \left(\frac{\sigma_0}{\sigma_b}\right)^2 \right); \quad \rho_y = \frac{1}{2} \left( \left(\frac{2\sigma_0}{\sigma_{45}}\right)^2 - \left(\frac{\sigma_0}{\sigma_b}\right)^2 \right) \tag{13}$$

where  $\sigma_0$ ,  $\sigma_{45}$  and  $\sigma_{90}$  are the unidirectional yield stresses of 0, 45 and 90° relative to the rolling direction (RD). The stress  $\sigma_b$  is known as the biaxial yield stress determined by a biaxial tensile test experiment. It is worth noting that all these variants imply  $\sigma_{ref} = \sigma_0$ .

**b2- r-value-based Hill48's criterion (Hill48-r):** In this case, the plastic potential function requires three experimental uniaxial Lankford *r values*, corresponding to the rolling (0°), transverse (90°) and diagonal (45°) directions. The plastic potential function related to the experimental *r-value* s is given by:

$$\lambda_p = \frac{1 + 1/r_{90}}{1 + 1/r_0}; \quad \nu_p = \frac{1}{1 + 1/r_0}; \quad \rho_p = \frac{(1 + 2r_{45})(1/r_0 + 1/r_{90})}{2(1 + 1/r_0)} \tag{14}$$

where the  $r_0$ ,  $r_{45}$  and  $r_{90}$  Lankford parameters are the anisotropic ratios corresponding to the uniaxial tension test at 0°, 45°, and 90° orientations relative to the RD of the plane sheet.

### 3.2 Yld2000-2d Yield Criteria

Barlat et al.(Barlat et al., 2003) introduced a consistent and flexible exponential nonquadratic model for orthotropic and anisotropic materials, which was very successful for steel sheets. Equation (15) demonstrates the *Yld2000-2d* yield formalism in terms of the principal stress deviator tensor:

$$\begin{cases} \Phi = \Phi' + \Phi'' = 2\sigma_0^k \\ \Phi' = |S'_1 - S'_2|^k \\ \Phi'' = |2S''_2 + S''_1|^k + |2S''_1 + S''_2|^k \end{cases} \tag{15}$$

$\Phi'$  and  $\Phi''$  are two isotropic functions in the equations (two linear transformations),  $\sigma_0$  is the equivalent stress and “ $k$ ” is a constant of material that is mostly associated with the crystal structure behavior ( $k=8$  for a fcc and  $k=6$  for bcc materials), where the first and second modified principal deviatoric values are  $S'_{1,2}$  and  $S''_{1,2}$  in the plane sheet and can be shown as:

$$\begin{cases} S'_{1,2} = \frac{1}{2}(S'_{11} + S'_{22}) \pm \frac{1}{2}\sqrt{(S'_{11} - S'_{22})^2 + 4S'^2_{12}} \\ S''_{1,2} = \frac{1}{2}(S''_{11} + S''_{22}) \pm \frac{1}{2}\sqrt{(S''_{11} - S''_{22})^2 + 4S''^2_{12}} \end{cases} \tag{16}$$

For the anisotropic behavior,  $S'_{ij}$  and  $S''_{ij}$  are the linear transformation functions of the deviatoric stress tensor, which can be reduced to:

$$\begin{bmatrix} S'_{11} \\ S'_{22} \\ S'_{12} \end{bmatrix} = \begin{bmatrix} L'_{11} & L'_{12} & 0 \\ L'_{21} & L'_{22} & 0 \\ 0 & 0 & L'_{66} \end{bmatrix} \begin{bmatrix} s_{11} \\ s_{22} \\ s_{12} \end{bmatrix}, \quad \begin{bmatrix} S''_{11} \\ S''_{22} \\ S''_{12} \end{bmatrix} = \begin{bmatrix} L''_{11} & L''_{12} & 0 \\ L''_{21} & L''_{22} & 0 \\ 0 & 0 & L''_{66} \end{bmatrix} \begin{bmatrix} s_{11} \\ s_{22} \\ s_{12} \end{bmatrix} \tag{17}$$

The tensors  $L'$  and  $L''$ , which describe linear stress tensor transformations, are as follow:

$$L_{ij} = \begin{bmatrix} L_{11} & L_{12} & L_{13} & 0 & 0 & 0 \\ L_{21} & L_{22} & L_{23} & 0 & 0 & 0 \\ L_{31} & L_{32} & L_{33} & 0 & 0 & 0 \\ 0 & 0 & 0 & L_{44} & 0 & 0 \\ 0 & 0 & 0 & 0 & L_{55} & 0 \\ 0 & 0 & 0 & 0 & 0 & L_{66} \end{bmatrix} \stackrel{\text{Sheet plane}}{=} \begin{bmatrix} L_{11} & L_{12} & 0 \\ L_{21} & L_{22} & 0 \\ 0 & 0 & L_{66} \end{bmatrix}$$

For convenience in the calculation of the anisotropy parameters, the coefficients of  $L'$  and  $L''$  can be expressed by relationships of a set of eight coefficients  $\alpha_1$  to  $\alpha_8$ , as follows:

$$L' = \begin{bmatrix} L'_{11} \\ L'_{12} \\ L'_{21} \\ L'_{22} \\ L'_{66} \end{bmatrix} = \begin{bmatrix} \frac{2}{3} & 0 & 0 \\ -\frac{1}{3} & 0 & 0 \\ 0 & -\frac{1}{3} & 0 \\ 0 & \frac{2}{3} & 0 \\ 0 & 0 & 1 \end{bmatrix} \begin{bmatrix} \alpha_1 \\ \alpha_2 \\ \alpha_7 \end{bmatrix}, \quad L'' = \begin{bmatrix} L''_{11} \\ L''_{12} \\ L''_{21} \\ L''_{22} \\ L''_{66} \end{bmatrix} = \frac{1}{9} \begin{bmatrix} -2 & 2 & 8 & -2 & 0 \\ 1 & -4 & -4 & 4 & 0 \\ 4 & -4 & -4 & 1 & 0 \\ -2 & 8 & 2 & -2 & 0 \\ 0 & 0 & 0 & 0 & 9 \end{bmatrix} \begin{bmatrix} \alpha_3 \\ \alpha_4 \\ \alpha_5 \\ \alpha_6 \\ \alpha_8 \end{bmatrix} \quad (18)$$

It is important to calibrate eight independent coefficients of anisotropy for the yield function. Note that the parameters will be reduced to unity ( $\alpha_1 = \alpha_2 = \dots = \alpha_8 = 1$ ) for the simple isotropic case of von Mises. The identification of these anisotropic coefficients was determined by eight material tensile tests ( $\sigma_0, \sigma_{45}, \sigma_{90}, \sigma_b, r_0, r_{45}, r_{90}$ , and  $r_b$  between yield stresses and  $r$ -values, respectively), where  $\sigma_b$  is the equibiaxial yield stress and  $r_b$  is the equibiaxial anisotropic coefficient. A nonlinear system is solved numerically employing the Newton-Raphson method to find parameters  $\alpha_{1-8}$ . The specimen axis is rotated by an angle  $\vartheta$  according to the rolling direction (RD). Furthermore, the stress and strain tensors in the uniaxial test are given as:

$$\begin{cases} \sigma_{11} = \sigma(\theta) \cos^2 \theta \\ \sigma_{22} = \sigma(\theta) \cos^2 \theta \\ \sigma_{12} = \sigma(\theta) \sin \theta \cos \theta \end{cases} \quad (19)$$

where  $\sigma_{11}, \sigma_{22}$ , and  $\sigma_{12}$  are components of the stress tensor in the specimen under the uniaxial tensile test. The  $r$ -value parameter can be computed from the following equation:

$$r(\theta) = \frac{\dot{\epsilon}_{yy}}{\dot{\epsilon}_{zz}} = - \frac{\left(\frac{f(\sigma_{ij})}{\partial \sigma_{11}}\right) \cdot \sin^2 \theta - \left(\frac{f(\sigma_{ij})}{\partial \sigma_{12}}\right) \cdot \sin 2\theta + \left(\frac{f(\sigma_{ij})}{\partial \sigma_{22}}\right) \cdot \cos^2 \theta}{\frac{f(\sigma_{ij})}{\partial \sigma_{11}} + \frac{f(\sigma_{ij})}{\partial \sigma_{22}}} \quad (20)$$

where  $f(\sigma_{ij}) = \left(\frac{\Phi}{2}\right)^{1/k} = \left(\frac{\Phi' + \Phi''}{2}\right)^{1/k}$

The equibiaxial Lankford parameter is  $r_b = \epsilon_{yy}/\epsilon_{xx}$  (such as  $\epsilon_{yy}$ , which is the true strain in the transverse direction and  $\epsilon_{xx}$ : is the strain in the rolling directions), and this parameter is similar to the  $r$ -value. The application result of the same load in both rolling and transverse directions  $\sigma_b$  ( $\sigma_{xx} = \sigma_{yy}$ ) produces a strain gradient between the two stresses characterized by  $r_b$ . The equibiaxial coefficient reduces to a simple isotropic case for  $r_b$  equal to the unity.

Three ways can be proposed to determine this parameter:

1. Experimental (performing compression tests or equibiaxial tensile tests);
2. Microtextural discretization from a polycrystal model;
3. Theoretically using *Yld96* (Barlat et al., 1997) yield function.

In this work, the parameter  $r_b$  can be computed by the formulation proposed as below:

$$r_b = \frac{[-\alpha_x(c_3 + 2c_1)(2c_1 + c_2)|2c_1 + c_2|^{a-2} + \alpha_y(c_3 - c_1)(c_1 + 2c_2)|c_1 + 2c_2|^{a-2} - (2c_3 + c_1)(c_1 - c_2)|c_1 - c_2|^{a-2}]}{[-\alpha_x(c_2 - c_3)(2c_1 + c_2)|2c_1 + c_2|^{a-2} - \alpha_y(2c_2 + c_3)(c_1 + 2c_2)|c_1 + 2c_2|^{a-2} + (c_2 + 2c_3)(c_1 - c_2)|c_1 - c_2|^{a-2}]} \quad (21)$$

where the nonquadratic exponent  $\alpha$  is a material's constant and has the same meaning as 'k' for *Yld2000-2d*. The parameters of anisotropy  $c_1, c_2, c_3, \alpha_x$  and  $\alpha_y$  can be determined by the numerical solution using the Newton-Raphson method.

### 3.3 Yield function BBC2005 formulation

Another different analytical expression entitled the *BBC2000* (Banabic–Balan–Comsa) function was suggested on the basis of the isotropic formalism developed by Hershey (Hershey, 1954). These authors succeeded in developing a flexible formulation, called *BBC2005* (Banabic et al., 2005), by changing the eight coefficients of its earlier version. This formulation includes 8 coefficients of anisotropy, and consequently, the calibration procedure uses 8 mechanical characterizations (3 yield stresses:  $\sigma_0, \sigma_{45}$  and  $\sigma_{90}$ , 3 uniaxial parameters of *r-values*,  $r_0, r_{45}$  and  $r_{90}$ , the equibiaxial yield stress  $\sigma_b$  and the equibiaxial coefficient  $r_b$ ). The equivalent yield function is defined as follows:

$$\sigma_0 = \left[ a(\Delta + \Gamma)^{2\chi} + a(\Delta - \Gamma)^{2\chi} + b(\Delta + \Psi)^{2\chi} + b(\Delta - \Psi)^{2\chi} \right]^{\frac{1}{2\chi}} \quad (22a)$$

where the nonquadratic exponential  $\chi \in \mathbb{N}^{\geq 1}$  and material parameters  $a, b > 0$ , but the  $\Gamma, \Delta$  and  $\Psi$  functions depend on the planar components of the stress tensor as follows:

$$\begin{cases} \Gamma = L\sigma_{11} + M\sigma_{22} \\ \Delta = \sqrt{(N\sigma_{11} - P\sigma_{22})^2 + \sigma_{12}^2} \\ \Psi = \sqrt{(Q\sigma_{11} - R\sigma_{22})^2 + \sigma_{12}^2} \end{cases} \quad (22b)$$

The  $a, b, L, M, N, P, Q, R$  and  $\chi$  material parameters define the size and shape of the function given in Equation (23a). For the best prediction of the *BBC2005* yield criterion, these coefficients should be positive values according to the numerical tests performed by the authors. Six constants are obtained using a different solicitation in longitudinal tests. The latter must be complemented by other experiments, such as compression tests, which used to obtain the equibiaxial  $r$  value and a hydraulic bulge test to characterize the equibiaxial yield stress (Lăzărescu et al., n.d.). From these parameters, the  $\chi$  integer exponent has a special status. It is a nonquadratic parameter  $\chi=3$  for bcc metals and  $\chi=4$  for fcc alloys.

$$\sigma(\theta) = \frac{\sigma_0}{f(\theta)} \quad (23a)$$

Where

$$f(\theta) = \left[ a(\Delta_\theta + \Gamma_\theta)^{2\chi} + a(\Delta_\theta - \Gamma_\theta)^{2\chi} + b(\Delta_\theta + \Psi_\theta)^{2\chi} + b(\Delta_\theta - \Psi_\theta)^{2\chi} \right]^{\frac{1}{2\chi}} \quad (23b)$$

And

$$\begin{cases} \Gamma_{\theta} = L \cos^2 \theta + M \sin^2 \theta \\ \Delta_{\theta} = \sqrt{(N \cos^2 \theta - P \sin^2 \theta)^2 + \cos^2 \theta \sin^2 \theta} \\ \psi_{\theta} = \sqrt{(Q \cos^2 \theta - R \sin^2 \theta)^2 + \cos^2 \theta \sin^2 \theta} \end{cases} \quad (23c)$$

The uniaxial plastic *r-value*  $r(\theta)$  formulation was evaluated from Equation (24):

$$r(\theta) = \frac{[f(\theta)]^{2\chi}}{G(\theta)} - 1 \quad (24)$$

Where

$$\begin{aligned} G(\theta) = & a \left[ \frac{(N-P)(N \cos^2 \theta - P \sin^2 \theta)}{\Delta_{\theta}} + L + M \right] (\Delta_{\theta} + \Gamma_{\theta})^{2\chi-1} + \\ & + a \left[ \frac{(N-P)(N \cos^2 \theta - P \sin^2 \theta)}{\Delta_{\theta}} - L - M \right] (\Delta_{\theta} - \Gamma_{\theta})^{2\chi-1} + \\ & + b \left[ \frac{(N-P)(N \cos^2 \theta - P \sin^2 \theta)}{\Delta_{\theta}} + \frac{(Q-R)(Q \cos^2 \theta - R \sin^2 \theta)}{\psi_{\theta}} \right] (\Delta_{\theta} + \psi_{\theta})^{2\chi-1} + \\ & + b \left[ \frac{(N-P)(N \cos^2 \theta - P \sin^2 \theta)}{\Delta_{\theta}} - \frac{(Q-R)(Q \cos^2 \theta - R \sin^2 \theta)}{\psi_{\theta}} \right] (\Delta_{\theta} - \psi_{\theta})^{2\chi-1} \end{aligned}$$

The theoretical coefficient of biaxial plastic anisotropy is calculated as follows:

$$r(b) = \frac{[f(b)]^{2\chi}}{G(b)} - 1 \quad (25)$$

where

$$f(b) = \left[ a(\Delta_b + \Gamma_b)^{2\chi} + a(\Delta_b - \Gamma_b)^{2\chi} + b(\Delta_b + \psi_b)^{2\chi} + b(\Delta_b - \psi_b)^{2\chi} \right]^{\frac{1}{2\chi}}$$

$$\begin{aligned} G(b) = & a \left[ \frac{N(N-P)}{\Delta_b} + L \right] (\Delta_b + \Gamma_b)^{2\chi-1} + a \left[ \frac{N(N-P)}{\Delta_b} - L \right] (\Delta_b - \Gamma_b)^{2\chi-1} + \\ & + b \left[ \frac{L(N-P)}{\Delta_b} + \frac{Q(Q-R)}{\psi_b} \right] (\Delta_b + \psi_b)^{2\chi-1} + b \left[ \frac{N(N-P)}{\Delta_b} - \frac{Q(Q-R)}{\psi_b} \right] (\Delta_b - \psi_b)^{2\chi-1} \end{aligned}$$

**\*Calibration for the Yld200-2d and BBC2005 Yield Functions**

To evaluate the mechanical anisotropy of sheet metals, both the *Yld2000-2d* and *BBC2005* functions incorporated 8 anisotropic coefficients. These anisotropic coefficients are identified as follows:

- For Associated Flow Rule

Eight unknown anisotropy coefficients of both yield functions were obtained using eight experimental material datasets (four yield stresses,  $\sigma_0, \sigma_{45}, \sigma_{90}$  and  $\sigma_b$ , as well as four *r-value* s,  $r_0, r_{45}, r_{90}$  and  $r_b$ ). The anisotropy parameters of the nonlinear system can be determined by the numerical solution using the Newton-Raphson method.

- For Non-Associated Flow Rule

Eight yield stresses,  $\sigma(\vartheta)$  ( $\vartheta = 0^\circ, 15^\circ, 30^\circ, 45^\circ, 60^\circ, 75^\circ, 90^\circ$ ) and  $\sigma_b$ , for yield function  $\sigma(\vartheta)$  as well as eight  $r(\vartheta)$ -values (for seven orientations,  $\vartheta = 0^\circ, 15^\circ, 30^\circ, 45^\circ, 60^\circ, 75^\circ, 90^\circ$ ) and  $r_b$ , for the plastic potential were obtained. The anisotropic parameters of the *Yld200-2d* and the *BBC2005* yield functions under the nonassociated flow rule were calibrated using the well-known nonlinear Levenberg-Marquardt least-square algorithm implemented in *MATLAB<sup>TM</sup>* software.

The difference between the predicted and experimental results for yield stresses and  $r$ -values was calculated from error functions as follows:

$$\text{Error (stress)} = \text{Error}(\sigma_{(\theta)}) + \text{Error}(\sigma_b).$$

$$\text{Error}_{\sigma_{(\theta)}} = \frac{1}{2} \sum_{i=1}^t [\sigma_i^{\text{theo}}(\theta) - \sigma_i^{\text{exp}}(\theta)]^2, \quad \text{Error}_{\sigma_b} = \frac{1}{2} \sum_{i=1}^t [\sigma_b^{\text{theo}} - \sigma_b^{\text{exp}}]^2$$

$$\text{Error (r-value)} = \text{Error}(r_{(\theta)}) + \text{Error}(r_b) \tag{26}$$

$$\text{Error}_{r_{(\theta)}} = \frac{1}{2} \sum_{i=1}^t [r_i^{\text{theo}}(\theta) - r_i^{\text{exp}}(\theta)]^2, \quad \text{Error}_{r_b} = \frac{1}{2} \sum_{i=1}^t [r_b^{\text{theo}} - r_b^{\text{exp}}]^2$$

The number of available experimental data points employed in the calculations was mentioned by “ $t$ ”. The subscript ‘*theo*’ indicates the predicted value given by *Yld2000-2d* and *BBC2005*, so ‘*exp*’ indicates the experimental characterization.

## 4 COMPARISON OF EXPERIMENTAL AND MODELED (PREDICTED) RESULTS

### 4.1 Microstructural Parameter Identification of Ferritic Stainless Steels at the initial state

The material used in this study is a FS Steel X3CrTi17 (known as AISI 439-430Ti; NE 1.4510) sheet of 1 mm thickness. A comprehensive description including the preparation and heat treatment of such a material as well as the tensile testing procedure can be found in more detail in a previous work(O. Chahaoui et al., 2013).

#### a. Conditions for Image Analysis

The modification of flow stresses during plastic deformation is usually known as strain hardening, from which the minimizing of deformation work contributes to obtain these stresses. However, the work hardening is simply defined as an increasing of the stress beyond a material's internal resistance plastic flow, with the rising of plastic strain. Thus, the stress state remains on the growing yield surface, even though the shape and size of the surface may change as plastic deformation evolves. Thereby, for the reason of the gradual evolution of the crystallographic texture, the topological arrangement of the different constituents and phases is strongly revealed.

In this context, in order to refine the understanding about the mechanical behavior of ferritic stainless steel at the macroscopic scale, it is first worth to provide quantitative information on grain features and their arrangement, at the mesoscopic scale through the image analysis. Thus, based on the digital image two-dimensional (2D) analysis, such parameters are usually obtained from optical microscope. Automated image segmentation (classical image segmentation is described as the image division into regions of interest (ROIs)) has frequently proven to produce reasonable results, noting that it is sometimes less successful when dealing with highly irregular and/or elongated grains(Bunge et al., 2000; Fonseca et al., 2009; R. Hill, 1990).

The optical microstructures treated hereby were already described earlier(O. Chahaoui et al., 2013) as being in an annealed state (revealed at 50  $\mu\text{m}$  of observation scale) through the three orthotropic planes of the sheet. Image analysis was evaluated to verify the effectiveness of the 2D segmentation technique that relies on the threshold operation.

The image processing of the micrographs consisted of two steps; the first step consisted of reducing the noise by using a “despeckle” filter and then converting the image into an 8-bit image. The second step used the distribution of gray levels to determine a threshold value from the Otsu algorithm. The result of the segmentation is presented in Figure 2, where the colors represent grain morphological orientations relative to the X direction. This orientation is calculated by fitting an approximated ellipse over the grain, from which the angle is calculated as the difference between the major diameter and the X-axis(Fonseca et al., 2009).

For the material and technology considered here, simple thresholding was found to be insufficient to separate the grain boundaries. Another solution was to use Trainable Weka Segmentation Plugin (Houtte et al., 1989) with ImageJ Software. For the present study, two states were considered: grains and grain boundaries. A one-pixel sized pen tool was used for the feature selection of each state to allow the maximum accuracy. This is due to the thin nature of grain boundaries at this scale of observation. The selected features are Gaussian blur, Sobel filter, Hessian, difference of Gaussians and membrane projections.

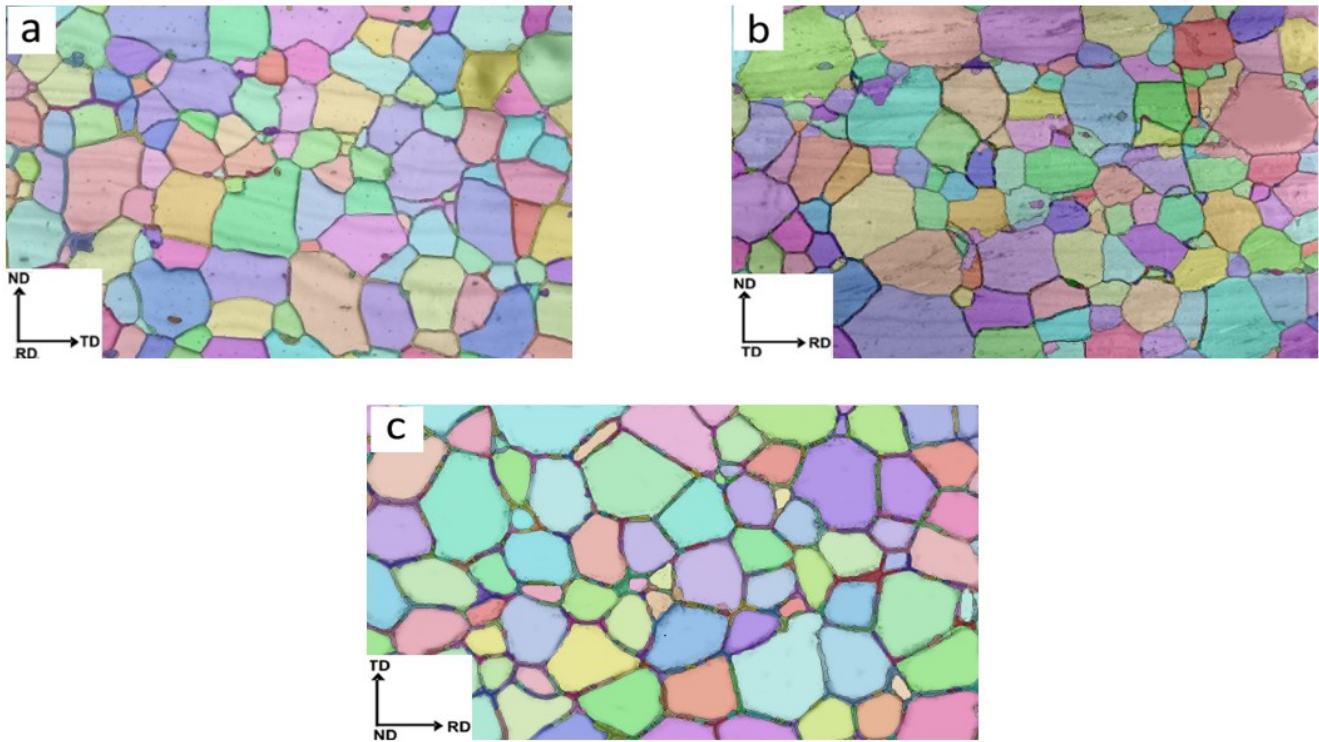


**Figure 2** Morphological textures produced by segmentation processing in orthotropic plan (a) (TD, ND), (b) (RD, ND), (c) (RD, TD) of Ferritic Stainless Steels microstructures at initiate state (Colour figures on the online version).

**Table 1** Calculated mean of area, aspect ratio and angle distribution and with respective 95% confidence Intervals.

Measured microstructural parameters from Orthotropic Plans			
	Optical image analysed in (TD, ND)	Optical image analysed in (RD, ND)	Optical image analysed in (RD, TD)
Area ( $\mu\text{m}^2$ )	$416.727 \pm 79.845$	$417.974 \pm 78.358$	$326.429 \pm 68.093$
AR	$1.804 \pm 0.185$	$1.681 \pm 0.158$	$1.754 \pm 0.121$
Angle ( $^\circ$ )	$79.753 \pm 8.319$	$74.348 \pm 8.257$	$66.728 \pm 7.354$

**b. Microstructure quantitative description**

At first glance, it can be easily observed that via the three planes, and from a morphological perspective, the microstructures exhibit almost identical homogenous trends, which correspond to a typical state of an annealed steel and common uncompleted recrystallization. However, a quantitative analysis was modeled using a cumulative density function (CDF) and a Probability density function (PDF). It is well observed that some small differences along the three planes, especially for the area distribution (Figure 3(a) and (b)), grain aspect ratio distribution (Figure 4(a) and (b)), and grain morphological angle (Figure 5(a) and (b)).

For the grain area distribution, the (RD, TD) plane exhibited a reduced average grain size, i.e., approximately 22% smaller (Table 1), with a tight spread, and only 21% of grains (Figure (3a)) are larger than  $500 \mu\text{m}^2$  compared to  $\approx 32\%$  for the other planes. The aspect ratio (AR) describes the elongation of the grains, which is calculated by dividing the largest diameter  $d_{\text{max}}$  over the smallest orthogonal diameter  $d_{\text{min}}$ . For an annealed ferritic steel, the aspect ratio should be 1 or close to 1. The average ratio (AR) of the three microstructures ranges from 1.68 to 1.8 with similar distributions, and only a small fraction of the grains, approximately 13.8%, have AR values close to 1; these values are also observed in the literature (Wang et al., 2006).

The distribution angle shows a similar trend, where for the (RD, TD) plane, there is a preferential orientation at approximately 20°, where 35% of the grains have an angle of 20° or less, whereas for the (TD, ND) and (RD, ND) planes, only 13% and 16% have such an angle, respectively, and both show a more uniform angle distribution compared to the (RD, TD) planes. It is important to observe that this orientation distribution along (RD, TD) coincides with the formation of crystallographic fibers during cold rolling. This is often observed in the case of ferritic steels, in which the maximum texture is generally found on the alpha fiber, close to  $\{112\}$ //RD orientations and the dominant texture components, namely, (111) [341] located along the so-called gamma-fibers ( $\{111\}$ //ND)(O. Chahaoui et al., 2013; Martinez et al., 2001).

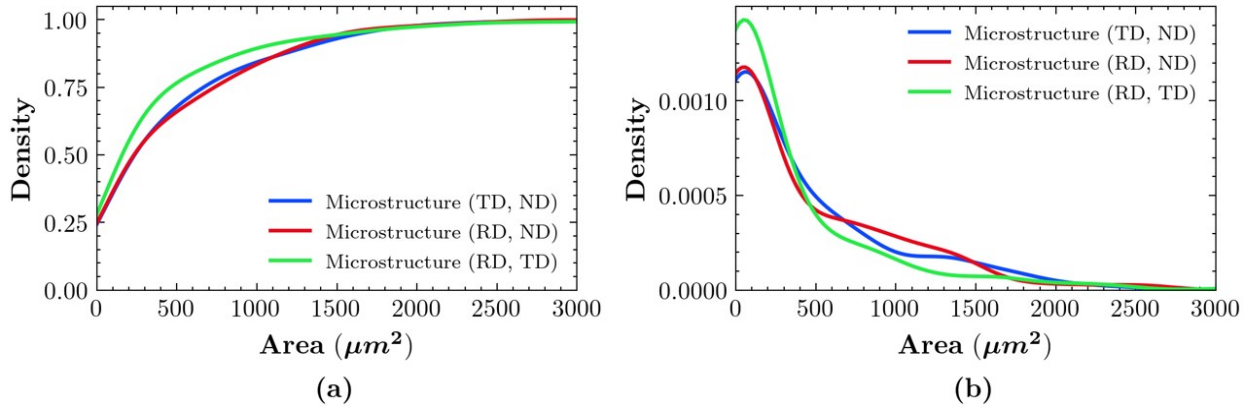


Figure 3 (a) Cumulative density function (CDF) and (b) Probability density function (PDF) of grain area distribution in the three orthotropic planes.

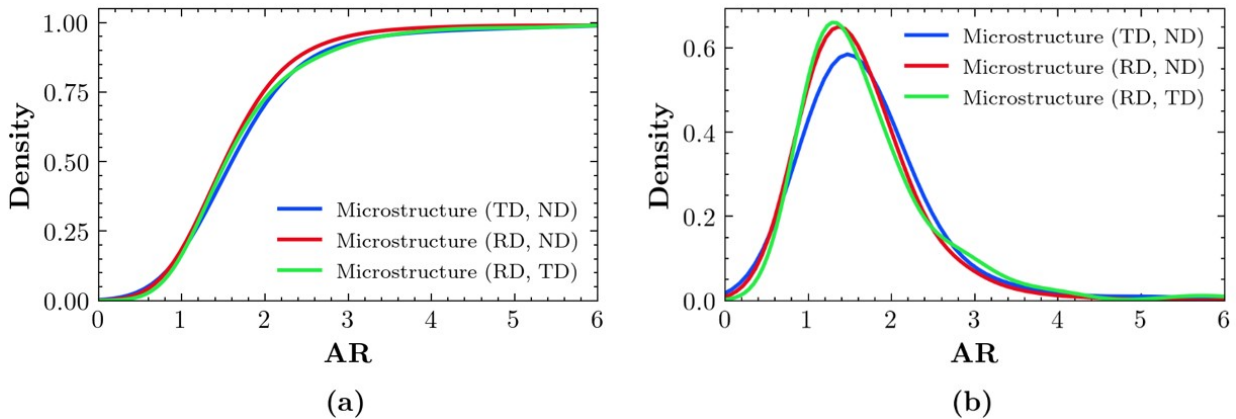


Figure 4 (a) Cumulative density function (CDF) and (b) Probability density function (PDF) of grain aspect ratio distribution in the three orthotropic planes.

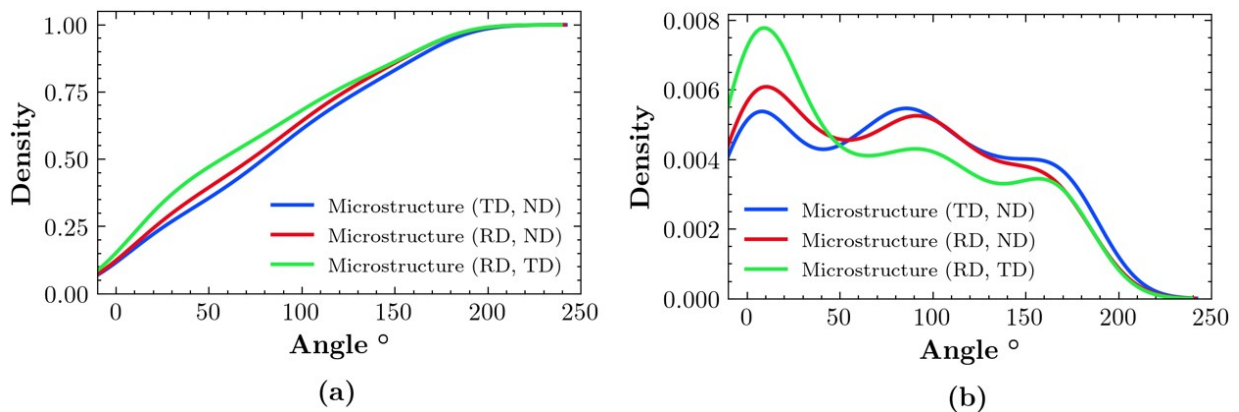


Figure 5 (a) Cumulative density function (CDF) and (b) Probability density function (PDF) of the grain morphological orientation distribution in the three orthotropic planes.

### 4.2 Uniaxial Tensile Test

The experimental parameters of the overall sheet, especially the  $\sigma(\vartheta)$  yield stress and the  $r(\vartheta)$  Lankford value, were determined through uniaxial tensile tests. The sheet specimen was held at orientations of  $0^\circ$  relative to RD,  $15^\circ$ ,  $30^\circ$ , and  $45^\circ$  relative to DD, and  $60^\circ$ ,  $75^\circ$  and  $90^\circ$  relative to TD. Note that the specimen has a negative value of planar anisotropy  $\Delta r = (r_0 - 2 r_{45} + r_{90})/2 = -0.65$ . Moreover, an average Lankford coefficient  $\bar{r} = (r_0 + 2 r_{45} + r_{90})/4 = 1.085$  for 9% of plastic deformation (above unity) reflects the better formability of this steel. Both equibiaxial parameters, such as the biaxial yield stress ( $\sigma_b$ ) and biaxial Lankford  $r$ -value ( $r_b$ ), should also be determined. In this investigation, because the anisotropic behavior of the sheet metal is not highly sensitive to equibiaxial stress, the balanced biaxial stress was assumed to equal unity ( $\sigma_b = 1$ ); however, ( $r_b$ ) greatly affects plastic anisotropy and was computed using the *Yld96* yield function (Barlat et al., 1997). To calibrate the *Yld96* yield criteria, seven parameters ( $\sigma(0^\circ)$ ,  $\sigma(45^\circ)$ ,  $\sigma(90^\circ)$ ,  $r(0^\circ)$ ,  $r(15^\circ)$ ,  $r(90^\circ)$ ) were evaluated to predict the biaxial stress ( $r_b$ ) and were equal to 0.8612. The results are shown in Table 2. For the 17% prestrain stage, the mechanical elastoplastic parameters of this rolled sheet were already computed.

**Table 2** Mechanical Properties for FS Steel along seven directions

$\vartheta$	$\theta^\circ$	$\sigma_{e0.2}$ (MPa)	$\sigma_b$ (MPa) <sup>a</sup>	$r(\theta)$	$r_b$	$\bar{r}$	$\Delta r$
0.3	$0^\circ$	278		0.7	0.8612	1.085	-0.65
	$15^\circ$	270		0.9			
	$30^\circ$	272		1.26			
	$45^\circ$	283	278	1.41			
	$60^\circ$	260		1.30			
	$75^\circ$	277		1.24			
	$90^\circ$	271		0.82			

<sup>a</sup> the equibiaxial yield stress  $\sigma_b$  was assumed:  $\sigma_b = \sigma_{e0.2}$

From Table 2, it is worth noting that the  $r(\vartheta)$  Lankford parameter increases from 0.7 to 1.41 along orientations in the range of  $[0, 45^\circ]$  and decreases from 1.30 to 0.82. Note that with  $\Delta r$  close to -0.65, the value was far from zero ( $\Delta r \neq 0$ ), and it greatly favors the occurrence of the earing steel; thus, it does not lead to an extra-deep drawing quality. Similar results have been reported previously by *Martinez et al.* (Martinez et al., 2001).

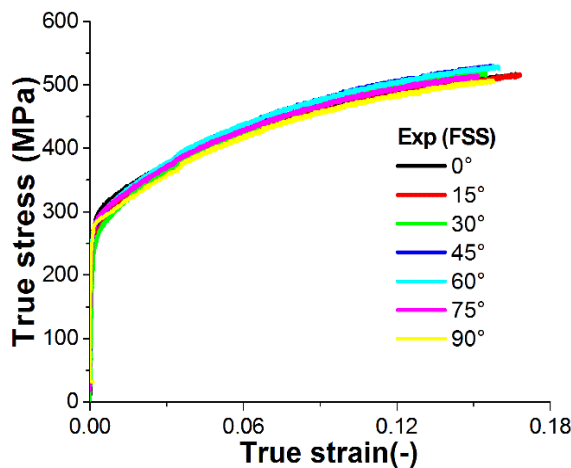


**Figure 6** Experimental uniaxial Stress-Strain curves of ferritic stainless steel (FSS)(Oualid Chahaoui, 2011).

Figure 6 shows the experimental unidirectional stress-strain curves from the as-received sheet for seven specimens extracted in its plane(Oualid Chahaoui, 2011). For reproducibility, three rectangular uniaxial specimens of 1 mm thickness, 7 mm width and 30 mm gauge length were used (O. Chahaoui et al., 2013).

The mechanical parameters (yield stress and  $r$ -value) normalized with respect to their initial values for various directions are shown in Table 3.

**Table 3** The normalized uniaxial tensile test of yield stress and *r*-value.

	$\frac{\sigma_0}{\sigma_0}$	$\frac{\sigma_{15}}{\sigma_0}$	$\frac{\sigma_{30}}{\sigma_0}$	$\frac{\sigma_{45}}{\sigma_0}$	$\frac{\sigma_{60}}{\sigma_0}$	$\frac{\sigma_{75}}{\sigma_0}$	$\frac{\sigma_{90}}{\sigma_0}$	$\sigma_b$
Yield stress	1	0.974	0.981	1.021	0.936	0.998	0.977	1
	$\frac{r_0}{r_0}$	$\frac{r_{15}}{r_0}$	$\frac{r_{30}}{r_0}$	$\frac{r_{45}}{r_0}$	$\frac{r_{60}}{r_0}$	$\frac{r_{75}}{r_0}$	$\frac{r_{90}}{r_0}$	$r_b$
<i>r</i> -value	1	1.285	1.8	2.01	1.85	1.77	1.17	0.8612

the equibiaxial yield stress  $\sigma_b$  was assumed  $\sigma_b = 1$  and the  $r_b$ -value was calculated from *Yld96* (Barlat et al., 1997)

### 4.3 Hardening characterization of FSS

The formula of flow stress is related to the uniaxial stress-strain results to describe the mechanical behaviour of the strain path of ferritic stainless steel. It is shown that a good fit is achieved first by Voce, which was a more appropriate choice of stress-strain evolution of prestrained material (Figure 7). This isotropic hardening function is generally expressed by the Voce hardening formulation in Equation (27):

$$\sigma_t = \sigma_{Sat} - (\sigma_{Sat} - \sigma_0) \exp(-\beta \varepsilon_t) \tag{27}$$

where  $\sigma_0$  is a reference stress and  $\sigma_{sat}$  and  $\beta$  are material parameters to be calibrated. To compute the values of the theoretical yield stress-strain relations, it is mandatory to calculate the saturation stress  $\sigma_{sat}$  and hardening coefficient  $\beta$  by solving nonlinear curve-fitting (data-fitting) problems in a least-squares sense by minimizing the error estimation of each equation:

$$\min_x = \sum_{i=1} [(F(x, xdata_i) - ydata_i)]^2 \tag{28}$$

here *xdata* and *ydata* are the input data and the corresponding observed output data, respectively. The saturation stress  $\sigma_{sat}$  and hardening coefficient  $\beta$  were obtained by the fitting data (true stress, true strain) in the uniaxial tensile test along the seven directions. The results are presented in Table 4 as below.

**Table 4** Fitting data for Voce hardening law

Test Direction	Voce Law	
	$\sigma_{sat}$ [MPa]	$\beta$
0°	539.83	13.15
15°	512.17	19.72
30°	542.72	15.26
45°	554.75	14.5
60°	549.45	15.08
75°	547.68	13.30
90°	545.57	12.08

Figures 7 and 8 show the reproduced longitudinal tensile curves according to the rolling direction RD and for specimens extracted at 7 different directions based on the Voce hardening model, respectively.

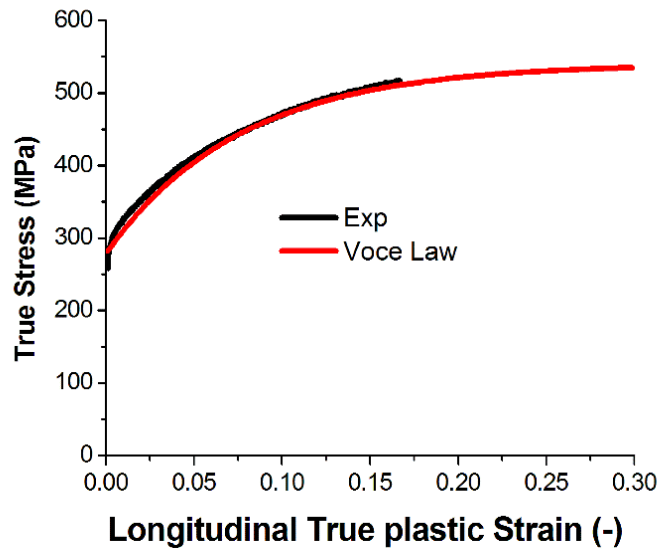


Figure 7 Fitting of experimental hardening curve with Voce hardening model according to RD.

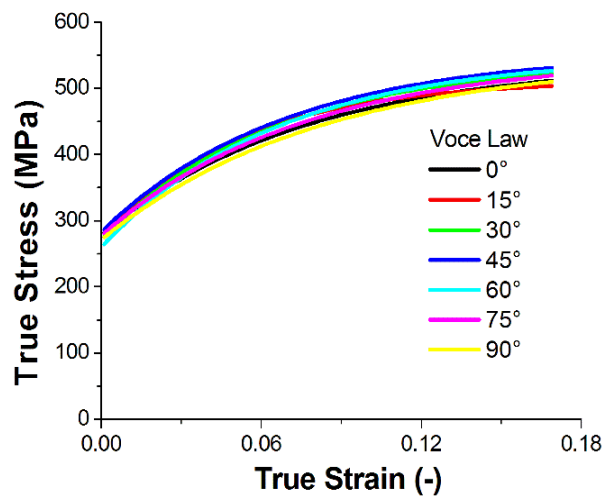


Figure 8 Directional uniaxial curves for FSS in terms of true strain in seven orientations.

4.4 Evaluation of initial anisotropy coefficients for the three yield criteria

Analytical and numerical characterization results values of all independent anisotropy parameters of three Hill48, Yld2d-2000, BBC2005 functions for as-received material are summarized in Tables 5 to 7 as:

a- Initial anisotropy coefficients of Yld2000-2d and BBC2005 under AFR.

Table 5 Identification of all independent anisotropy coefficients under AFR approach

	$\alpha_1$	$\alpha_2$	$\alpha_3$	$\alpha_4$	$\alpha_5$	$\alpha_6$	$\alpha_7$	$\alpha_8$
Yld 2000-2d	0.9151	1.0417	0.9146	1.0125	1.0267	1.0015	1.0123	0.8797
	$a$	$b$	$L$	$M$	$N$	$P$	$Q$	$R$
BBC2005	0.4293	0.6683	0.5470	0.4787	0.5166	0.5149	0.3931	0.4235

b- Calculated anisotropy coefficients identified under NAFR.

1. Initial anisotropy coefficients of three functions based on yield stress ( $\sigma$ ).

**Table 6** Identification of all independent anisotropy coefficients under NAFR-y approach

Hill48	$\lambda$		$\nu$				$\rho$	
	1.0476		0.5238				-0.0164	
Yld 2000-2d	$\alpha_1$	$\alpha_2$	$\alpha_3$	$\alpha_4$	$\alpha_5$	$\alpha_6$	$\alpha_7$	$\alpha_8$
	0.4894	1.373	1.2575	1.0035	-0.965	-0.555	-0.003	1.7066
BBC2005	$a$	$b$	$L$	$M$	$N$	$P$	$Q$	$R$
	0.3001	0.2655	1.0289	0.0037	0.1698	0.2490	0.1587	0.9991

2. Initial anisotropy coefficients of three functions based on plastic potential (*r-values*).

**Table 7** Identification of all independent anisotropy coefficients under NAFR-r approach

Hill48	$\lambda$		$\nu$				$\rho$	
	0.943		0.441				0.1441	
Yld 2000-2d	$\alpha_1$	$\alpha_2$	$\alpha_3$	$\alpha_4$	$\alpha_5$	$\alpha_6$	$\alpha_7$	$\alpha_8$
	0.5207	0.6805	0.6826	0.6984	0.7355	0.5620	0.7359	1.0810
BBC2005	$a$	$b$	$L$	$M$	$N$	$P$	$Q$	$R$
	0.0473	2.3648	1.0155	1.0965	0.4044	0.0414	0.4535	0.7187

The predicted mechanical parameters ( $\sigma(\vartheta)$  and  $r(\vartheta)$ ) of the three *Hill48*, *Yld2000-2d* and *BBC2005* formulations and experimental data at different material orientations are shown in Figure 9, based on two approaches of plasticity (*AFR* and *non-AFR*). However, from the previous, it was concluded that from:

- Figure 9(a), the *Hill48* criteria and the *Yld2000-2d* and *BBC2005* models under *AFR* assumption do not predict well the experimental behavior of  $\sigma(\vartheta)$  in the sheet plane.
- Figure 9(b), the *Hill48* criteria under *NAFR* assumption gives more advantage to better predict Lankford parameter in comparison with the *Yld2000-2d* and *BBC2005* models under *AFR* assumption.
- Figures 9 (c, d) and under *NAFR* reference, the *Yld2000-2d* and *BBC2005* models are able to capture the  $\sigma(\vartheta)$  and  $r(\vartheta)$  trends in an acceptable manner.

The analysis of this section clearly shows that provide sufficient flexibility and accuracy to approximate the uniaxial yield stress and plastic potential, respectively.

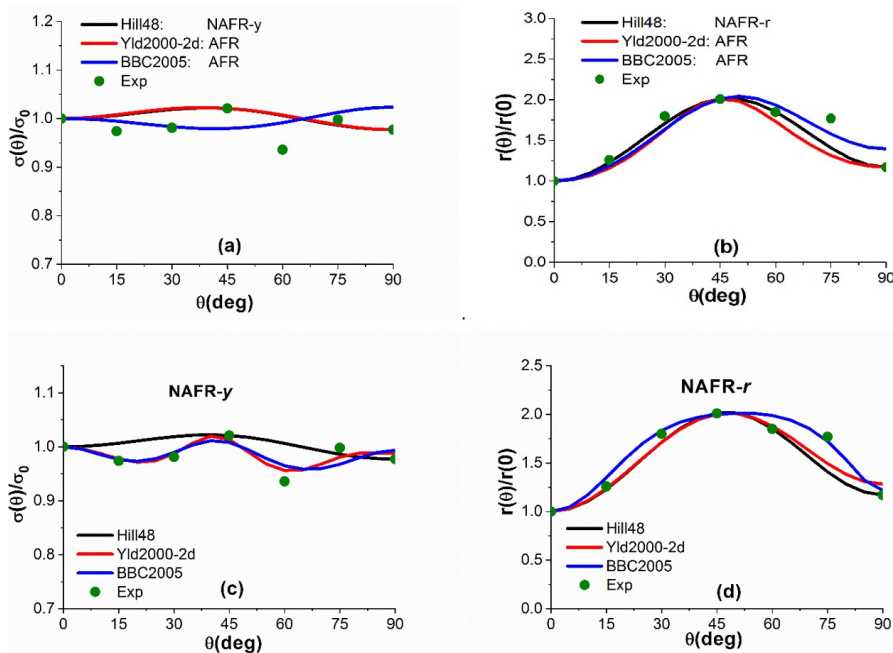


**Figure 9** Normalized yield stress and Lankford coefficient of three yield curves predicted with *Hill48*, *Yld-2000-2d*, *BBC2005* and Experiment behavior under *AFR* in (a), (b), and *non-AFR* approach in (c) and (d).

### 4.5 Impact of shear stress and comparison of yield surfaces

In order to compare the flow surface with anisotropic yield stress and to illustrate the high distortion of the yield surface for these *FSS* sheet specimens, the normalized shear stress is displayed by its isovalue contours. Figure 10 depicts the yield locus of the *Hill48*, *Yld2000-2d* and *BBC2005* functions and expressed as isoshear contours of the stress ratio  $\sigma_{12} / \sigma_0 = 0, 0.1, 0.2, 0.3, 0.4$  plotted in the sheet plane ( $\sigma_{11} / \sigma_0, \sigma_{22} / \sigma_0$ ), which were ( $\sigma_{11} = \sigma_{RD}, \sigma_{22} = \sigma_{TD}$ ).

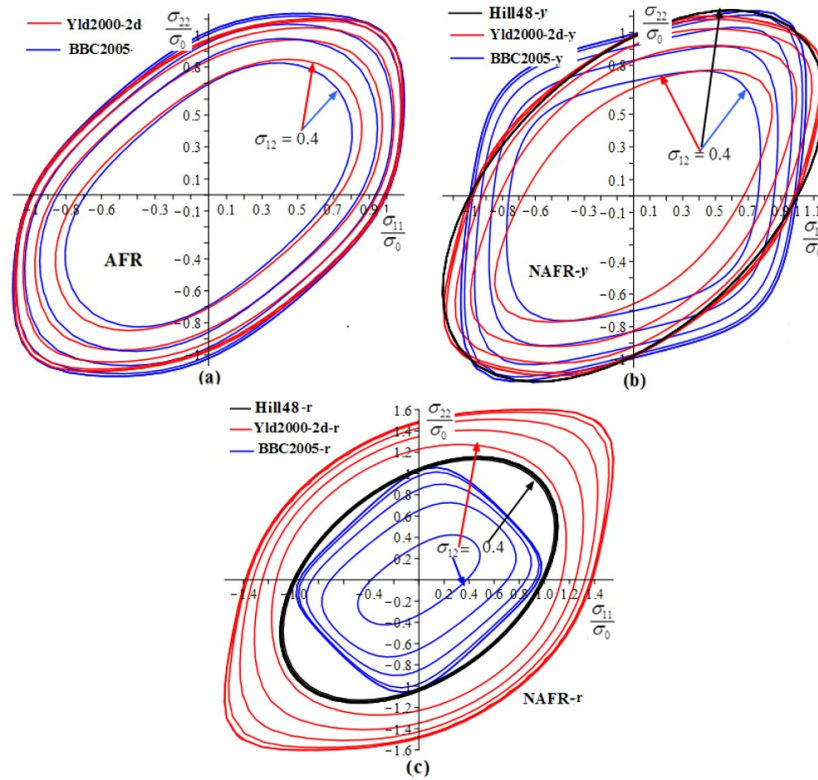


**Figure 10** The calculated yield surface represented by contours of the normalized shear stress at every 0.1 based on the *Hill48*, *Yld2000-2d* and *BBC2005* yield functions (a) Associated Flow Rule, (b) Non-Associated Flow Rule (yield functions) (c) Non-Associated Flow Rule (plastic potentials).

It is worth noting that the shape size of the two-dimensional sections of the yield surfaces appears to be influenced under the associated and nonassociated flow rule approaches. The following observations must be pointed out:

- i) The significant impact of shear stress  $\sigma_{12}$  on the behavior of stainless steel, shown in Figure 10(a), (b) and (c), was reported in the two nonquadratic criteria (*Yld2000-2d* and *BBC2005*) under the consideration of the two assumptions of plasticity. In addition, a negligible impact is noted for the *Hill48* model, as depicted in Figure 10(b) and (c).
- ii) A remarkable trend towards the expansion of the flow surface predicted by the *BBC2005* criterion in the direction of pure shear  $\sigma_{11}/\sigma_0 = -\sigma_{22}/\sigma_0$  is shown in Figure 10(b). However, a severe contraction of the same function is observed in the *NAFR-r* approach (Figure 10(c)).
- iii) Generally, the shear stress value is often equal to 60% of the yield flow stress  $\sigma_0$  in the uniaxial tensile test. Thus, it is recommended to experimentally characterize the sheet by a shear test to determine the real value of  $\sigma_{12}$ .

Table 8 presents the theoretical impact of the shear stress value at these two extreme values ( $\sigma_{12}=0$  and  $\sigma_{12}=0.4$ ) in the sheet metal plane ( $\sigma_{11}/\sigma_0, \sigma_{22}/\sigma_0$ ) for the three yield functions and under consideration of the two approaches. it should be noted that:

- a) For  $\sigma_{12}=0$ .
  - i) The maximum impact of  $\sigma_{12}$  is found on  $\sigma_{22}/\sigma_0$  for the *Yld2000-2d* criterion followed by  $\sigma_{11}/\sigma_0$  under the *NAFR-r* assumption.
  - ii) The minimum impact is depicted for  $\sigma_{11}/\sigma_0$  for the *BBC2005* yield criterion under the *NAFR-r* approach.

b) For  $\sigma_{12}=0.4$ .

j) The maximum impact of  $\sigma_{12}$  is found on  $\sigma_{22}/\sigma_0$  for the *Yld2000-2d* criterion under the *NAFR-r* assumption.

jj) The minimum impact is depicted for  $\sigma_{22}/\sigma_0$  in the *BBC2005* yield criterion under the *NAFR-r* approach.

**Table 8** Theoretical impact of shear stress value.

Function	Stress	$\sigma_{12}=0$			$\sigma_{12}=0.4$		
		AFR	NAFR-y	NAFR-r	AFR	NAFR-y	NAFR-r
Hill48	$\sigma_{11}/\sigma_0$	/	0.989	0.855	/	0.989	0.855
	$\sigma_{22}/\sigma_0$	/	1.021	1.052	/	1.021	0.998
Yld2000-2d	$\sigma_{11}/\sigma_0$	0.962	1.029	1.393	0.724	0.748	0.888
	$\sigma_{22}/\sigma_0$	1.028	0.985	1.509	0.747	0.725	1.121
BBC2005	$\sigma_{11}/\sigma_0$	0.965	0.893	0.636	0.665	0.585	0.432
	$\sigma_{22}/\sigma_0$	1.023	1.095	0.676	0.726	0.732	0.344

**5 DETERMINATION AND EVOLUTION OF MECHANICAL PARAMETERS: LANKFORD  $r(\theta)$  AND YIELD STRESS  $\sigma(\theta)$ .**

The most common parameter used to characterize the anisotropy behaviour was the Lankford coefficient (also called the *r(θ)-value*). The latter is defined as the true strain ratio of the transverse and thickness directions characterized in the uniaxial tensile test specimen. Since materials strongly resist volume changes, this parameter is often computed based on the incompressibility hypothesis. The definition of the *r-value* can be presented as follows:

$$r(\theta)_{\text{instantaneous}} = \frac{\varepsilon_w(\theta)}{\varepsilon_t(\theta)} \Rightarrow \frac{\varepsilon_2(\theta)}{\varepsilon_3(\theta)} = \frac{\varepsilon_2(\theta)}{-(\varepsilon_1(\theta) + \varepsilon_2(\theta))} = -\frac{m(\theta)}{1 + m(\theta)} \quad \text{with} \quad \varepsilon_1(\theta) + \varepsilon_2(\theta) + \varepsilon_3(\theta) = 0 \quad (29)$$

where  $\varepsilon_1$ ,  $\varepsilon_2$  and  $\varepsilon_3$  are the true plastic deformations along the longitudinal, transverse and thickness directions measured from uniaxial tensile tests of metal or alloy specimens, respectively. The relation between the transverse and longitudinal true plastic strains is noted by the slope  $m(\theta)$ , which is obtained by the linear regression of the fitted curve. The technique utilized to calculate the Lankford parameter was based on the method outlined in the *British Standard BS ISO 10113:2006* according to Kilpatrick et al. (Kilpatrick et al., 2010). The obtained transverse versus longitudinal true plastic strain curves are plotted in Figure 11 for all seven specimens with different orientations.

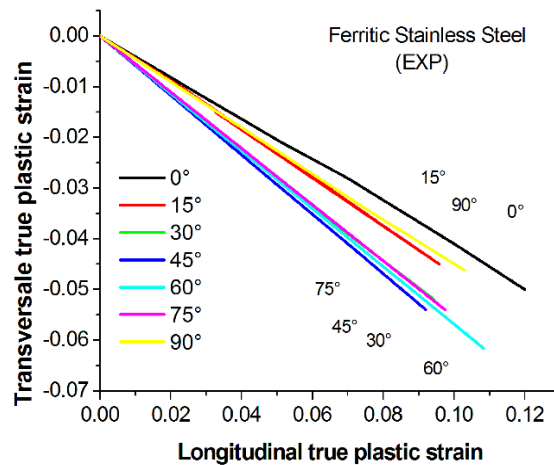


**Figure 11** The experimental plastic flow ratios of uniaxial tensile tests of FSS.

The gradient  $m(\theta)$  represents the slope of the straight line of both parameters of transverse and longitudinal true plastic strain, as shown in figure 11. The evolution of the experimental Lankford coefficient along the seven directions is estimated from the linear regression of the following first-degree polynomials:

$$\varepsilon_2(\theta) = a + m(\theta)\varepsilon_1(\theta) \tag{30}$$

The explicit results of the ratios between the transverse to longitudinal true plastic strain and by considering the use of relations (29) and (30), the experimental evolving parameters for seven orientations are provided in Table 9.

**Table 9** Parameters of linear fit

Angle	$a$	$m(\theta)$
0°	0.0002	-0.414
15°	0.0004	-0.4715
30°	0.000006	-0.5574
45°	0.00002	-0.5863
60°	0.00001	-0.5677
75°	0.000003	-0.5545
90°	-0.00006	-0.4499

In this investigation, based on Voce model optimization of the experimental uniaxial tensile curve in the rolling direction, the range of a dataset is proposed between the lowest (0.001) and the highest (0.3) values of longitudinal plastic strain  $\varepsilon_{11}^p$  with a step of 0.05. Only constant values of Lankford parameters are presented in figure 11 using a linear regression, but to compute the instantaneous  $r$ -value, (Lee et al., 2017; Safaei et al., 2013; Safaei, Lee, et al., 2014) suggested a 3<sup>rd</sup> order polynomial to the ratio of transverse to longitudinal plastic strains as follows:

$$\text{Poly3}(\bar{\varepsilon}^p) = a_1(\bar{\varepsilon}^p)^3 + a_2(\bar{\varepsilon}^p)^2 + a_3(\bar{\varepsilon}^p) + a_4 \tag{31}$$

In plastic behavior and for better modeling, the directional longitudinal plastic strain  $\varepsilon_{11}^p$  is assumed to be equal to the equivalent plastic strain  $\bar{\varepsilon}^p$ . Furthermore, the evolution of the instantaneous anisotropic coefficient of the three *Hill48*, *Yld2000-2* and *BBC2005* functions under both approaches is evaluated. The parameters of the 3<sup>rd</sup> order polynomial fit (*Poly3*) for all seven orientations are presented in Table 10.

**Table 10** Parameters of Poly3.

Angle	$a_1$	$a_2$	$a_3$	$a_4$
0°	-4.5904	0.6178	-0.4254	0.00006
15°	3.3284	-0.7086	-0.4321	0.00002
30°	5.6472	-0.6116	-0.5427	-0.00005
45°	-1.8540	0.2238	-0.592	0.00002
60°	0.1930	-0.441	-0.5652	-0.00001
75°	0.4280	-0.0632	-0.5523	-0.000004
90°	2.5938	-0.3112	-0.4439	-0.00002

Figure 12 depicts the experimental results of normalized yield stress  $\sigma(\vartheta)$  and the anisotropic coefficient ratio  $r(\vartheta)$  in terms of longitudinal equivalent plastic strain amount dependence for seven tested orientations in the sheet plane. Representative mechanical features of  $\sigma(\vartheta)$  and  $r(\vartheta)$  obtained by extrapolating the adopted Voce hardening model for the strain range  $0.001 \leq \bar{\varepsilon}^p \leq 0.3$ . The instantaneous change in the normalized flow stress is more pronounced at approximately 7.5% of the longitudinal equivalent strain amounts, and then it stabilizes, with a certain singularity for the 15° orientation. For the

experimental Lankford coefficient, the dependence over the complete range of deformation levels is significantly high throughout all directions with the exception of 30°, 60° and 75°, where the dependence is nearly monotonous. The instantaneous variation of mechanical characteristics as a function of the proportions evolution of the equivalent deformation ranging from 0 to 0.3 in the 7 directions are presented in Appendix A. II (Table A. II. 1 and Table A. II. 2, respectively). The mechanical proprieties  $\sigma(\vartheta)$  and  $r(\vartheta)$  have been Instantly evolved during the deformation proportions.

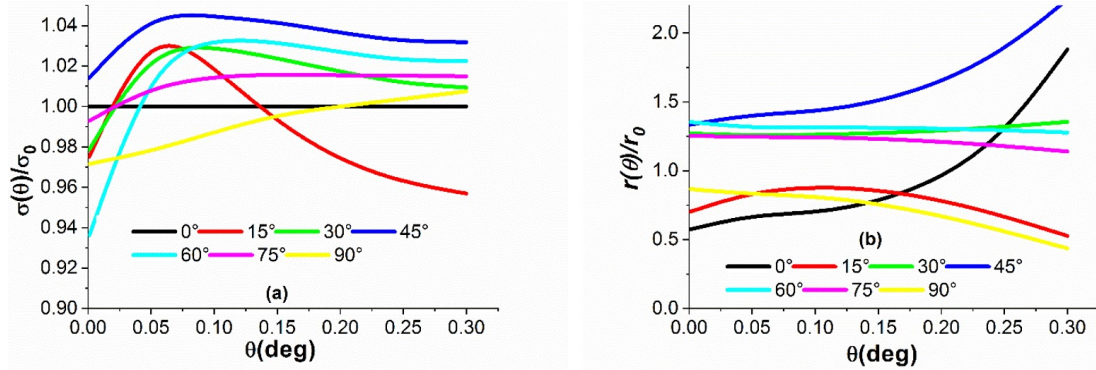


**Figure 12** Equivalent plastic strain dependence of the experimental mechanical parameters corresponding to selected orientations: (a) Normalized yield stress distribution and (b) Lankford coefficient distribution.

Figure 13 shows the evolution of the experimental mechanical parameters corresponding to the selected  $\bar{\epsilon}^p$  in the sheet plane. The different selected levels of plastic deformation have a significant impact on the sheet behavior represented by both mechanical parameters. The values of the normalized yield stress measured experimentally in all 7 directions coincide almost perfectly with the lowest amount (0.001) of  $\bar{\epsilon}^p$ . Generally, it is observed that a lower level of equivalent plastic strain results in higher values in terms of mechanical properties (data expressed in Table A.1.1 and Table A.1.2 from Appendix A. I).

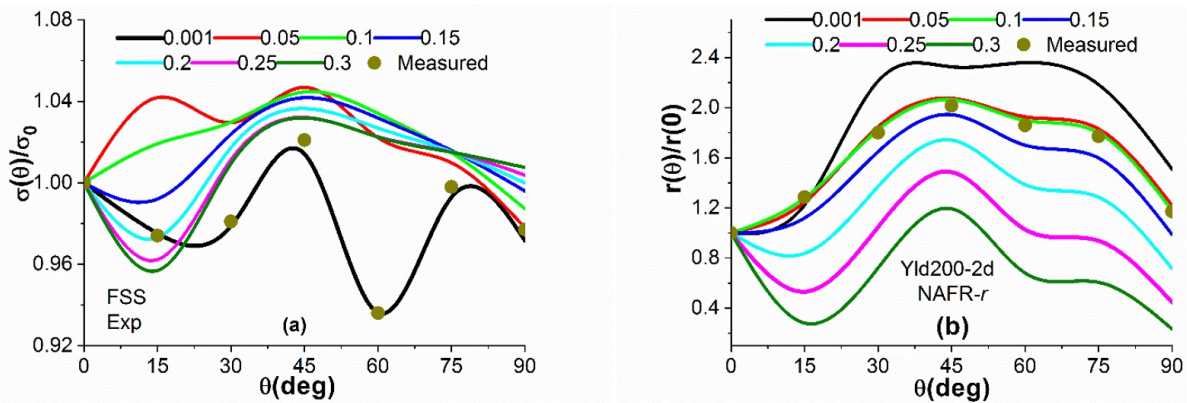


**Figure 13** Angular dependence of the experimental mechanical parameters corresponding to selected  $\bar{\epsilon}^p$  of (a) Normalized yield stress distribution and (b) Lankford coefficient distribution.

**5.1 Anisotropic estimation of evolutionary behavior under the nonassociated flow rule**

To estimate the evolving anisotropy behavior, two nonquadratic functions of *Yld2000-2d* and *BBC2005* are proposed. These functions are considered under the nonassociated flow rule to predict the directional dependence of yield stress ratios and *r-values* at seven orientations in a plane sheet 15° from the rolling direction RD (reference direction). Anisotropic parameters in the *Yld2000-2d* and *BBC2005* models were calibrated by minimizing the error function defined in Equation (31). The distribution of anisotropy parameters for both yield functions corresponding to selected true plastic strains was optimized for seven angles. The optimized parameters of the yield stress and *r-value* are summarized in Tables 11 and 12, respectively. It is important to note that the equibiaxial stress and the equibiaxial Lankford coefficient remained unchanged, which is similar to the results presented in previous sections.

**Table 11-a** Parameters of Yld2000-2d yield function (NAFR-y).

$\bar{\epsilon}^p$	$\alpha_1$	$\alpha_2$	$\alpha_3$	$\alpha_4$	$\alpha_5$	$\alpha_6$	$\alpha_7$	$\alpha_8$
0.001	0.4985	1.3871	1.2651	1.0007	-0.9631	-0.5536	-0.0124	1.7195
0.050	0.8223	0.9202	0.9575	1.0639	1.0197	0.8610	-0.0155	1.1674
0.100	0.9821	1.1229	1.0802	0.9540	0.9823	1.0456	0.8714	1.0428
0.150	0.8269	1.2699	1.6518	0.6506	1.0160	1.0131	1.0395	0.6092
0.200	-1.1256	1.9080	0.5901	-0.6533	1.0398	0.8888	0.9282	0.9966
0.250	-1.3359	1.9852	0.9285	-0.5693	0.8715	0.4756	0.9138	1.0689
0.300	-1.3656	1.9741	0.9317	-0.5689	0.8399	0.3505	0.9132	1.0947

**Table 11-b** Parameters of Yld2000-2d potential function (NAFR-r).

$\bar{\epsilon}^p$	$\alpha_1$	$\alpha_2$	$\alpha_3$	$\alpha_4$	$\alpha_5$	$\alpha_6$	$\alpha_7$	$\alpha_8$
0.001	1.1248	-0.3046	1.1151	0.5486	-0.0400	-0.8391	0.3363	1.0344
0.050	0.5988	0.6681	0.9720	0.7413	0.8084	0.5938	0.8178	1.1190
0.100	0.4895	0.5317	0.8353	0.6031	0.6635	0.4617	0.6767	0.9387
0.150	1.0912	-0.2578	0.9626	0.4823	-0.75e-2	-0.6549	0.3633	0.9283
0.200	1.1491	1.1354	-1.9999	0.5387	2.1664	4.1985	2.0737	2.7817
0.250	0.6701	-0.5219	1.9293	0.6835	2.2138	4.4174	2.2695	3.2205
0.300	-0.3024	1.0165	1.0543	0.5267	0.2329	-0.3588	0.4828	0.0677

**Table 12-a** Parameters of BBC2005 yield function (NAFR-y).

$\bar{\epsilon}^p$	$a$	$b$	$L$	$M$	$N$	$P$	$Q$	$R$
0.001	0.3381	0.2805	0.9997	0.0038	0.1782	0.2764	0.1476	0.9713
0.050	0.5788	0.3183	0.5273	0.3337	0.4092	0.6365	0.6812	0.4783
0.100	0.4186	0.3663	0.5835	0.2769	0.3735	0.6646	0.7273	0.4633
0.150	0.3959	0.3835	0.6450	0.3395	0.4155	0.5717	0.6207	0.5552
0.200	2.6448	0.2002	0.1839	0.2490	0.0014	0.4138	1.1700	0.8351
0.250	0.5213	0.2210	0.8715	0.0068	0.2483	0.4546	0.1434	0.8176
0.300	0.4880	0.1982	0.8925	0.0100	0.2398	0.4220	0.1172	0.8702

**Table 12-b** Parameters of BBC2005 potential function (NAFR-r).

$\bar{\epsilon}^p$	$a$	$b$	$L$	$M$	$N$	$P$	$Q$	$R$
0.001	2.0617	0.6840	0.4222	0.2382	0.0208	0.1538	0.5897	0.3835
0.050	1.9436	0.6899	0.4087	0.2609	0.0027	0.1311	0.6197	0.3904
0.100	0.0859	2.7094	0.9129	1.0156	0.3905	0.0465	0.4619	0.6958
0.150	1.3107	0.4332	0.3990	0.2533	0.0309	0.1312	0.6131	0.3698
0.200	0.0047	1.4515	0.6569	0.8862	0.0743	0.4788	0.6410	0.0764
0.250	0.7918	3.3402	0.8918	0.0004	0.1813	0.6906	0.1970	0.1392
0.300	3.9716	0.0002	0.0629	0.1801	0.1103	0.0730	1.0499	0.8891

Figure 14 shows the comparison between the angular dependence of the normalized anisotropic parameters (yield stress  $\sigma(\vartheta)$  and  $r$ -values  $r(\vartheta)$ ) predicted by the nonassociated flow rule *Yld2000-2d* and *BBC2005* models corresponding to the overall amounts of equivalent plastic strains. Under the *non-AFR* approach, the yield stress and the  $r$ -value function are independent. Almost all the predictions resulted in a good description of the normalized anisotropic parameters at the seven orientations. The *Yld2000-2d* model under the *NAFR-r* hypothesis better predicts the Lankford coefficients than the *BBC2005* model.

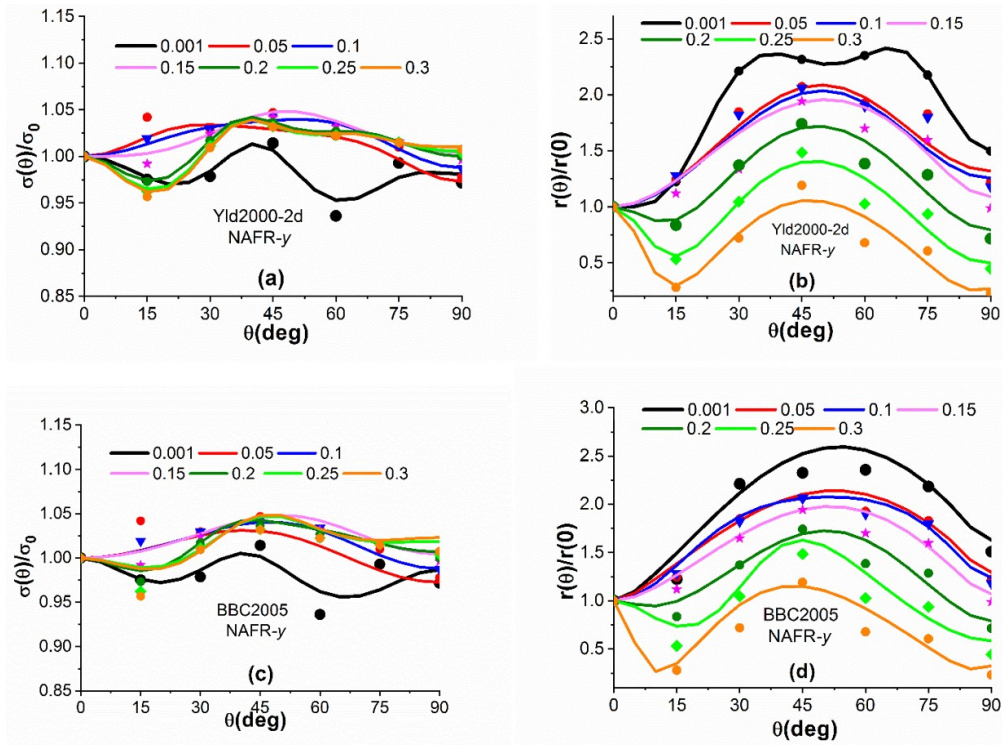


**Figure 14** Comparison between the angular dependence of the normalized anisotropic parameters  $\sigma(\vartheta)$  (a), (c) and  $r(\vartheta)$  in (b), (d) predicted by the *Yld2000-2d* and *BBC2005* models under *non-AFR* at overall intervals of equivalent plastic strains

Based on the isotropic hardening model of the Voce and 3<sup>rd</sup> order polynomial function, the historical surface evolution of anisotropic behavior associated with three amounts of equivalent deformation  $\varepsilon_{11}^p$  was captured on the sheet plane and on the normal plane space.

Figure 15 depicts the comparison between the contour surface evolution of the load locus and plastic potential of functions *Yld2000-2d* and *BBC2005* under *non-AFR* conditions at neglected shear stress  $\sigma_{12}=0$ . It can be observed that the shape and the evolution surface at each strain level of the yield stress surfaces are different from the plastic potential surfaces for both functions. This observation was recently cited by Lee and Safaei (Lee et al., 2017; Safaei, Lee, et al., 2014).

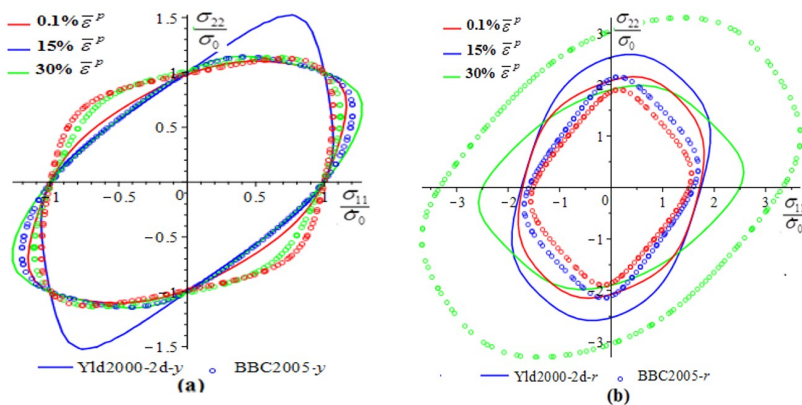


**Figure 15** Contour surfaces of evolutionary non-AFR *Yld2000-2d* and *BBC2005* functions corresponding to three levels of selected equivalent deformation at shear stress  $\sigma_{12}=0$ : (a) Yield Stress evolution and (b) Plastic potential evolution.

To incorporate the evolution of the yield stress  $\sigma(\vartheta)$  and *r-values*  $r(\vartheta)$  in a plane sheet 15° from the rolling direction RD, an appropriate polynomial fit is selected for both *non-AFR* evolving models. A fourth-order polynomial fit *Poly4* is adopted for the optimized anisotropy parameters of the *Yld200-2d* and *BBC2005* yield functions.

$$Poly4(\bar{\epsilon}^p) = a_1(\bar{\epsilon}^p)^4 + a_2(\bar{\epsilon}^p)^3 + a_3(\bar{\epsilon}^p)^2 + a_4(\bar{\epsilon}^p) + a_5 \tag{32}$$

The evolution history impact of the anisotropic properties during plastic deformation for the 7 directions of uniaxial tensile stress in the sheet plane was estimated. The mechanical behavior predicted under the *NAFR* hypothesis was performed using nonquadratic functions.

Steps were followed to capture anisotropic evolving nonassociated *Yld2000-2d* and *BBC2005* mechanical parameter models:

- i) Based on extrapolating the fit to Voce hardening model Equation (27), corresponding to the selected range of the equivalent plastic strain, the instantaneous evolution of the experimental normalized yield stress distribution was calculated.
- ii) From Equation (31), the 3<sup>rd</sup> order polynomial function (*Poly3*) of the linear regression to the ratio between the transverse and longitudinal plastic strains is used. As a result, the instantaneous *r-value* evolution was derived for all seven orientations. The balanced biaxial was assumed to be equal to the unity and biaxial Lankford *r-value*  $r_b=0.8612$  throughout the optimization procedure.
- iii) From Equation (32) and based on a 4<sup>th</sup> polynomial fit (*Poly4*), the anisotropic parameters of the yield function and plastic potential for both yield functions have been optimized and reported.

Each anisotropy parameter from 32 of the two nonquadratic criteria is a fourth- polynomial function under *non-AFR*.

Polynomial parameters based on fit curves are listed in Tables (A. II. 1, A. II. 2) and (A. II. 3, A. II. 4) (presented in Appendix A. II). Each anisotropy parameter from 32 of the two nonquadratic criteria is a fourth- polynomial function under *non-AFR* conditions.

Figures 16 and 17 show the prediction of the polynomial fit to the parameters in two functions for mechanical parameters. Exceptionally, the polynomial fits are mentioned for the anisotropic parameter  $\alpha_3$ , which exhibits singularity in terms of the proportions [0.15,0.2] of longitudinal true plastic strain under *NAFR-y* and the  $\alpha_2$  and  $\alpha_3$  values in terms of the proportions [0.15,0.20 and 0.25] under *NAFR-r*. On the other hand, generally, according to the *BBC2005* function predictions, the same comment is reported for the optimized parameters, such as (*b*, *N*) in the range of [0.05,0.1] and (*a*, *Q*) signaled at 0.2 in terms of proportions under *NAFR-y* and *NAFR-r*, respectively.

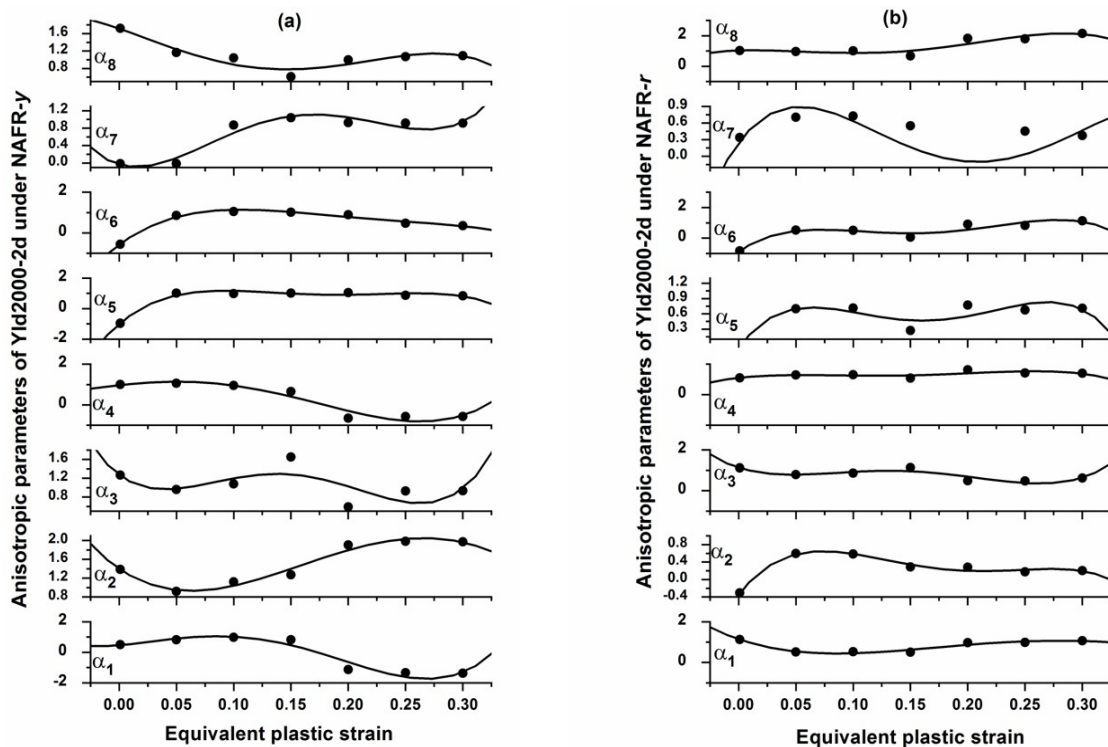


Figure 16 Polynomial fit (by Poly4) to the anisotropic parameters of *Yld2000-2d* under (a) *NAFR-y* and (b) *NAFR-r*.

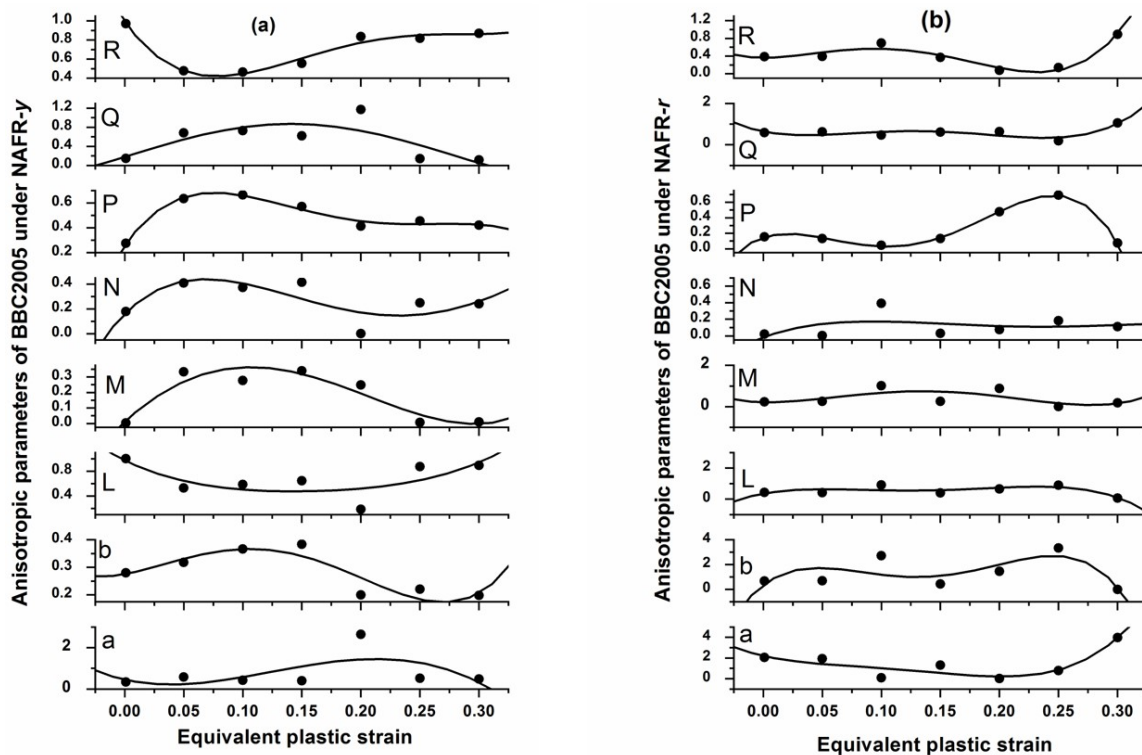


Figure 17 Polynomial fit (by Poly4) to the anisotropic parameters of *BBC2005* under (a) *NAFR-y* and (b) *NAFR-r*.

## 6 CONCLUSIONS

The importance of ferritic stainless steels in industrial applications is evident. Being able to correctly model their plastic behaviour is necessary in order to perform accurate simulations and use these materials at their full potential. For this purpose, the constitutive formulations based on the three orthotropic yield criteria of *Hill48*, *Yld2000-2d* and *BBC2005* were presented and analysed. From the modeled and experimental results, the main conclusions of the present study can be summarized as follows:

### 1. Regarding the initial anisotropy:

i) The conventional approach of the associated flow rule (AFR) was employed only for both nonquadratic *Yld2000-2d* and *BBC2005* functions, while the modern approach of the nonassociated flow rule was considered for three yield functions (*Hill48*, *Yld2000-2d* and *BBC2005*) to predict the directional dependence of mechanical parameters (normalized  $\sigma(\vartheta)$  and  $r(\vartheta)$ ) at the 7 different orientations selected.

ii) Under *non-AFR*, the *Yld2000-2d* and *BBC2005* nonquadratic models with more coefficients have provided enough flexibility to reasonably accurately describe the hardening curves from experimental uniaxial tests and Lankford coefficients. In addition, the yield flow surfaces were projected on the different values of the shear stress plane. The *BBC2005* criterion had a particular shape on surface contours, and on the other hand, it can be observed that nonvariation (no significant impact at shear stress) was reported for this steel under *NAFR* under the *Hill48* criterion.

### 2. Regarding the evolutionary anisotropy:

Two distinct paths of evolving history were considered under *non-AFR* using only the nonquadratic exponent yield criteria of *Yld2000-2d* and *BBC2005*. To capture anisotropic continuation changes, the evolution of the mechanical properties throughout a selected plastic deformation process was described:

i) For hardening anisotropy evolution and based on extrapolating the adopted Voce hardening model, the dependence and instantaneous evolution of the experimental normalized yield stress distribution corresponding to the selected range of the equivalent plastic strain was calculated.

- ii) For the Lankford  $r$ -value coefficient, the evolution of the transverse experimental to longitudinal plastic deformation ratio curves for 7 uniaxial directions using a 3rd polynomial fit (*Poly3*). The instantaneous  $r$ -value evolution was derived at a given  $15^\circ$  angle from the longitudinal to transverse direction. The effect of a particular level of equivalent deformation  $\epsilon_{11}^p$  on the changing surface history was presented employing only nonquadratic exponential yield criteria of *Yld2000-2d* and *BBC2005*.
- iii) The surface contours of the plastic potential and yield function were sensitively revealed with increasing plastic deformation.
- iv) The anisotropic parameters of both yield functions were identified and optimized using 4th- polynomial functions (*Poly4*).

## ACKNOWLEDGMENTS

The authors are indebted to Professor D. BRADAI and Dr B. MEHDI from USTHB Algiers as well as Dr N. KHERROUBA from CRTI-Algiers for their valuable advice and help in finalizing the document.

**Author's Contributions:** Conceptualization, O. Chahaoui, N. Matougui; Methodology, S. Boulahrouz; Investigation, O. Chahaoui, N. Matougui; Writing - original draft, O. Chahaoui, N. Matougui; Software, M.I.E Heddar, K. Babouri, S. Boulahrouz, Writing - review & editing, O. Chahaoui, N. Matougui; Validation, O. Chahaoui, N. Matougui, S Boulahrouz, M.I.E Hddar, K. Babouri; Resources, O. Chahaoui, N. Matougui; Supervision, O. Chahaoui, N. Matougui.

**Editor:** Marcílio Alves

## REFERENCES

- An, Y. G., Vegter, H., Melzer, S., and Romano Triguero, P. (2013). Evolution of the plastic anisotropy with straining and its implication on formability for sheet metals. *Journal of Materials Processing Technology* 213: 1419–1425.
- Banabic, D., Aretz, H., Paraianu, L., and Jurco, P. (2005). Application of various FLD modelling approaches. *Modelling and Simulation in Materials Science and Engineering* 13: 759–769.
- Banabic, D., Balan, T., and Comsa, D. S. (2000). A NEW YIELD CRITERION FOR ORTHOTROPIC SHEET METALS UNDER PLANE-STRESS CONDITIONS. In: *Proc. of 7th Cold Metal Forming Conference Cluj Napoca, Romania*, : 217–224.
- Banabic, D., Kuwabara, T., Balan, T., Comsa, D. S., and Julean, D. (2003). Non-quadratic yield criterion for orthotropic sheet metals under plane-stress conditions. *International Journal of Mechanical Sciences* 45: 797–811.
- Barlat, F., Aretz, H., Yoon, J. W., Karabin, M. E., Brem, J. C., and Dick, R. E. (2005). Linear transformation-based anisotropic yield functions. *International Journal of Plasticity* 21: 1009–1039.
- Barlat, F., Brem, J. C., Yoon, J. W., Chung, K., Dick, R. E., Lege, D. J., Pourboghrat, F., Choi, S.-H., and Chu, E. (2003). Plane stress yield function for aluminum alloy sheets—part 1: theory. *International Journal of Plasticity* 19: 1297–1319.
- Barlat, F., Maeda, Y., Chung, K., Yanagawa, M., Brem, J. C., Hayashida, Y., Lege, D. J., Matsui, K., Murtha, S. J., Hattori, S., Becker, R. C., and Makosey, S. (1997). Yield function development for aluminum alloy sheets. *Journal of the Mechanics and Physics of Solids* 45: 1727–1763.
- Belyakov, A., Miura, H., and Sakai, T. (1998). Dynamic recrystallization under warm deformation of a 304 type austenitic stainless steel. *Materials Science and Engineering: A* 255: 139–147.
- Benke, M., Hlavacs, A., Petho, D., Angel, D. A., Sepsi, M., Nagy, E., and Mertinger, V. (2018). A simple correlation between texture and earing. *IOP Conference Series: Materials Science and Engineering* 426: 012003.
- Beyerlein, I. J., and Knezevic, M. (2018). Review of microstructure and micromechanism-based constitutive modeling of polycrystals with a low-symmetry crystal structure. *Journal of Materials Research* 33: 3711–3738.

- Bron, F., and Besson, J. (2004). A yield function for anisotropic materials Application to aluminum alloys. *International Journal of Plasticity* 20: 937–963.
- Bunge, H. J., Pöhlndt, K., and Tekkaya, A. E. (2000). *Formability of Metallic Materials: Plastic Anisotropy, Formability Testing, Forming Limits*. Springer Science & Business Media.
- Chahaoui, O., Fares, M. L., Piot, D., and Montheillet, F. (2011). Monoclinic effects and orthotropic estimation for the behaviour of rolled sheet. *Journal of Materials Science* 46: 1655–1667.
- Chahaoui, O., Fares, M. L., Piot, D., and Montheillet, F. (2013). Mechanical modeling of macroscopic behavior for anisotropic and heterogeneous metal alloys. *Metals and Materials International* 19: 1005–1019.
- Chahaoui, Oualid. (2011). *Modélisation mécanique et l'étude expérimentale d'une tôle ferritique présentant des hétérogénéités texturales (gradient de texture et écart à l'orthotropie)*. Badji Mokhtar University of Annaba, Algeria.
- Cizek, P., and Wynne, B. P. (1997). A mechanism of ferrite softening in a duplex stainless steel deformed in hot torsion. *Materials Science and Engineering: A* 230: 88–94.
- Cvitanić, V., Kovačić, M., Cvitanić, V., and Kovačić, M. (2017). Algorithmic Formulations of Evolutionary Anisotropic Plasticity Models Based on Non-Associated Flow Rule. *Latin American Journal of Solids and Structures* 14: 1853–1871.
- Cvitanić, V., Vlák, F., and Lozina, Ž. (2008). A finite element formulation based on non-associated plasticity for sheet metal forming. *International Journal of Plasticity* 24: 646–687.
- Darbandi, P., and Pourboghrat, F. (2011). *An evolutionary yield function based on Barlat 2000 yield function for the superconducting niobium sheet*. : 210–217.
- Džoja, M., Cvitanić, V., Safaei, M., and Krstulović-Opara, L. (2019). Modelling the plastic anisotropy evolution of AA5754-H22 sheet and implementation in predicting cylindrical cup drawing process. *European Journal of Mechanics - A/Solids* 77: 103806.
- Fonseca, J., O'Sullivan, C., and Coop, M. R. (2009). Image Segmentation Techniques for Granular Materials. *AIP Conference Proceedings* 1145: 223–226.
- Hershey, A. V. (1954). The plasticity of an isotropic aggregate of anisotropic face-centered cubic crystals. *Journal of Applied Mechanics-Transactions of the Asme* 21: 241–249.
- Hill, R. (1990). Constitutive modelling of orthotropic plasticity in sheet metals. *Journal of the Mechanics and Physics of Solids* 38: 405–417.
- Hill, Rodney. (1948). A theory of the yielding and plastic flow of anisotropic metals. *Proceedings of the Royal Society of London. Series A. Mathematical and Physical Sciences* 193: 281–297.
- Houtte, P. V., Mols, K., Bael, A. V., and Aernoudt, E. (1989). APPLICATION OF YIELD LOCI CALCULATED FROM TEXTURE DATA. *Textures and Microstructures* 11: 23–3917.
- Hu, Q., Li, X., and Chen, J. (2018). On the calculation of plastic strain by simple method under non-associated flow rule. *European Journal of Mechanics - A/Solids* 67: 45–57.
- Karafillis, A. P., and Boyce, M. C. (1993). A general anisotropic yield criterion using bounds and a transformation weighting tensor. *Journal of the Mechanics and Physics of Solids* 41: 1859–1886.
- Kilpatrick, W., Brown, D., McMurray, R. J., and Leacock, A. G. (2010). The effect of serrated yielding on the determination of r-values in aluminium alloys and yield locus calibration. *Materials Science and Engineering: A* 527: 7557–7564.
- Lăzărescu, L., Comşa, D.-S., Nico, I., Ciobanu, I., and Banabic, D. (n.d.). Investigation of Bulge Radius Variation and its Effect on the Flow Stress in the Hydraulic Bulge Test. *Metal Forming* : 4.
- Lee, E.-H., Stoughton, T. B., and Yoon, J. W. (2017). A yield criterion through coupling of quadratic and non-quadratic functions for anisotropic hardening with non-associated flow rule. *International Journal of Plasticity* 99: 120–143.
- Lian, J., Shen, F., Jia, X., Ahn, D.-C., Chae, D.-C., Münstermann, S., and Bleck, W. (2018). An evolving non-associated Hill48 plasticity model accounting for anisotropic hardening and r-value evolution and its application to forming limit prediction. *International Journal of Solids and Structures* 151: 20–44.
- Martinez, V. J., Verdeja, J. I., and Pero-Sanz, J. A. (2001). Interstitial free steel Influence of a-phase hot-rolling and cold-rolling reduction to obtain extra-deep drawing quality. *Materials Characterization* : 9.

- Mises, R. v. (1913). Mechanik der festen Körper im plastisch- deformablen Zustand. *Nachrichten von der Gesellschaft der Wissenschaften zu Göttingen, Mathematisch-Physikalische Klasse* 1913: 582–592.
- Oh, G.-J., Lee, K.-M., Huh, M.-Y., Park, J. E., Park, S. H., and Engler, O. (2017). Effect of r-value and texture on plastic deformation and necking behavior in interstitial-free steel sheets. *Metals and Materials International* 23: 26–34.
- Raabe, D., and Lucke, K. (1993). *Textures of ferritic stainless steels*. 9: 11.
- Safaei, M., Lee, M.-G., Zang, S., and De Waele, W. (2014). An evolutionary anisotropic model for sheet metals based on non-associated flow rule approach. *Computational Materials Science* 81: 15–29.
- Safaei, M., Yoon, J. W., and De Waele, W. (2014). Study on the definition of equivalent plastic strain under non-associated flow rule for finite element formulation. *International Journal of Plasticity* 58: 219–238.
- Safaei, M., Zang, S., Lee, M.-G., and De Waele, W. (2013). Evaluation of anisotropic constitutive models: Mixed anisotropic hardening and non-associated flow rule approach. *International Journal of Mechanical Sciences* 73: 53–68.
- Spitzig, W. A., and Richmond, O. (1984). The effect of pressure on the flow stress of metals. *Acta Metallurgica* 32: 457–463.
- Stoughton, T. B. (2002). *The Influence of the Material Model on the Stress-Based Forming Limit Criterion*. : 2002-01–0157.
- Stoughton, T. B., and Yoon, J. W. (2006). Review of Drucker’s postulate and the issue of plastic stability in metal forming. *International Journal of Plasticity* 22: 391–433.
- Wang, W., Luo, W., and Tang, J. (2006). Particle Measurement by Image Processing and Analysis. *2006 International Conference on Computational Intelligence and Security* : 1861–1864.
- Zamiri, A., and Pourboghrat, F. (2007). Characterization and development of an evolutionary yield function for the superconducting niobium sheet. *International Journal of Solids and Structures* 44: 8627–8647.

**Appendix. A. I** Evolution of individual yield stresses and individual *r-values* corresponding to selected amounts of equivalent plastic strain are presented in Table A. I. 1 and Table A. I. 2 respectively.

**Table A. I. 1.** Evolution of individual normalized yield stresses  $\sigma(\vartheta)$  corresponding to selected  $\bar{\varepsilon}^p$ .

$\bar{\varepsilon}^p$	$\sigma(0^\circ)$	$\sigma(15^\circ)$	$\sigma(30^\circ)$	$\sigma(45^\circ)$	$\sigma(60^\circ)$	$\sigma(75^\circ)$	$\sigma(90^\circ)$
0.001	1	0.97518	0.97872	1.01418	0.93617	0.99291	0.97163
0.050	1	1.04187	1.02956	1.0468	1.02217	1.00985	0.97783
0.100	1	1.01915	1.02979	1.04468	1.03404	1.01489	0.98723
0.150	1	0.99205	1.02386	1.04175	1.03181	1.01591	0.99602
0.200	1	0.97313	1.01727	1.03647	1.02687	1.01536	1.00000
0.250	1	0.96226	1.01132	1.03208	1.02264	1.01509	1.00377
0.300	1	0.95693	1.00936	1.03184	1.02247	1.01498	1.00749

**Table A. I. 2** Evolution of individual normalized *r-values* corresponding to selected  $\bar{\varepsilon}^p$ .

$\bar{\varepsilon}^p$	$r(0^\circ)$	$r(15^\circ)$	$r(30^\circ)$	$r(45^\circ)$	$r(60^\circ)$	$r(75^\circ)$	$r(90^\circ)$
0.001	1	1.22418	2.211503	2.325108	2.358281	2.183799	1.508698
0.050	1	1.246607	1.847883	2.073169	1.926449	1.829988	1.219595
0.100	1	1.279115	1.822211	2.062573	1.89879	1.798216	1.179206
0.150	1	1.118716	1.648347	1.943499	1.700288	1.597507	0.986811
0.200	1	0.835771	1.370715	1.740996	1.385922	1.285746	0.714827
0.250	1	0.531437	1.046682	1.485406	1.027125	0.936483	0.445627
0.300	1	0.27997	0.720413	1.191991	0.679341	0.605906	0.231979

**Appendix. A. II** The polynomial parameters base on fit curves.

**Table A. II. 1** Parameters of *Poly4* (NAFR-y (Yld2000-2d)).

	$\alpha_1$	$\alpha_2$	$\alpha_3$	$\alpha_4$	$\alpha_5$
$\alpha_1$	3500.61394	-1564.77088	113.28182	6.43753	0.46411
$\alpha_2$	268.3796	-445.28563	170.65299	-16.48256	1.3996
$\alpha_3$	3038.5097	-1785.49476	317.95275	-17.68595	1.26855
$\alpha_4$	1214.90043	-355.90778	-39.49001	6.11028	0.96927
$\alpha_5$	-3428.1569	2491.05587	-628.78073	62.99631	-0.99002
$\alpha_6$	2698.69489	-1633.73345	282.36719	-7.27444	-0.03824
$\alpha_7$	2698.69489	-1633.73345	282.36719	-7.27444	-0.03824
$\alpha_8$	-907.72932	436.12011	-25.51277	-9.16293	1.71417

**Table A. II. 2** Parameters of *Poly4* (NAFR-r (Yld2000-2d)).

	$\alpha_1$	$\alpha_2$	$\alpha_3$	$\alpha_4$	$\alpha_5$
$\alpha_1$	1129.57486	-1163.550	320.107	-26.7825	1.17491
$\alpha_2$	740.34602	-17.30318	-112.23529	18.97449	-0.24487
$\alpha_3$	-5701.0074	3835.84153	-771.1828	41.43411	0.91096
$\alpha_4$	-1664.99198	1023.85176	-196.28808	11.66793	0.53589
$\alpha_5$	-10881.15632	5955.05145	-987.42368	54.97719	-0.0942
$\alpha_6$	-23183.24333	12359.38045	-1962.29577	103.91851	-0.94995
$\alpha_7$	-8686.87998	4619.72852	-725.85875	37.02929	0.29856
$\alpha_8$	-10834.59288	5416.13671	-760.63395	30.15909	0.9897

**Table A. II. 3** Parameters of *Poly4* (NAFR-y (BBC2005)).

	$\alpha_1$	$\alpha_2$	$\alpha_3$	$\alpha_4$	$\alpha_5$
<i>a</i>	190.82395	-567.43476	193.74051	-12.669	0.45586
<i>b</i>	317.33874	-149.91714	13.00691	0.79254	0.45586
<i>L</i>	321.47023	-205.95167	63.59246	-9.32993	0.97486
<i>M</i>	126.70179	5.51086	-36.42332	6.9587	0.01245
<i>N</i>	-310.68868	320.71803	-98.48892	9.39856	0.16177
<i>P</i>	-652.22189	522.88282	-141.62953	13.59903	0.25968
<i>Q</i>	390.52111	-218.83408	3.62922	7.6382	0.18064
<i>R</i>	688.65006	-597.58427	174.60464	-17.61809	0.99071

**Table A. II. 4** Parameters of *Poly4* (NAFR-r (BBC2005)).

	$\alpha_1$	$\alpha_2$	$\alpha_3$	$\alpha_4$	$\alpha_5$
<i>a</i>	4272.02031	-1872.07764	281.54511	-25.53195	2.20111
<i>b</i>	-11970.95013	6740.38578	-1183.85663	71.10276	0.36516
<i>L</i>	-2275.67263	1238.81553	-214.61907	13.46906	0.356
<i>M</i>	1720.26702	-958.35116	135.8374	-1.16877	0.21843
<i>N</i>	-169.13262	153.57264	-46.4759	5.18083	-0.0174
<i>P</i>	-2287.80031	1135.42997	-152.06592	4.96071	0.1465
<i>Q</i>	2446.25567	-1314.25155	214.51178	-10.86542	0.63652
<i>R</i>	1871.68384	-816.82443	82.31488	0.09804	0.36127